



NTNU
Norges teknisk-naturvitenskapelige universitet
Fakultet for naturvitenskap og teknologi
Institutt for kjemisk prosess teknologi

SPECIALIZATION PROJECT 2014

TKP 4550

PROJECT TITLE:

Modeling of Liquid-Liquid Subsea Separators

By

Preben Fürst Tyvold

Supervisor for the project: Sigurd Skogestad
Co-supervisor: Johannes Jäschke

Date:10.12.14

Abstract

The purpose of this project was to get an overview of the possibilities there are for subsea separation of oil and water and establish models for appropriate separators. The aim was to make the models suited for optimization and control purposes.

Models for a horizontal gravity separator and a co-current, in-line swirl separator was established and implemented in MATLAB. The models are based on characteristic droplet sizes and the separation rate is given by the the terminal velocity determined by the density difference between the dispersed and continuous phase and the frictional force given by Stoke's law. The swirl separator is modeled with an inner forced vortex and an outer free vortex, which determines the centrifugal force on the dispersed droplets as a function of the radial position.

In addition to oil and water, the models include asphaltene as a third component. The asphaltene distributions are modeled as simple, linear functions in the direction of separation. The influence of the asphaltenes on the oil-water separation rate is not included, but the models are meant to give an estimate for the accumulation of asphaltenes through a separation system.

Preface

This report presents work done as part of the specialization project (TKP4550) in the fifth year of the study program of MSc in Chemical Engineering at the Norwegian University of Science and Technology.

I would like to thank my supervisors, Professor Sigurd Skogestad and Associate Professor Johannes Jäschke, for their guidance and support through the project. I would also like to thank Associate Professor Brian A. Grimes for his help regarding population balances and the effect of asphaltenes on separation of emulsions.

Signature

Date

Contents

Abstract	i
Preface	ii
List of Figures	iv
List of Tables	iv
List of Symbols	iv
1 Introduction	1
2 Separation Theory	2
2.1 Principles of Separation Theory	2
2.1.1 Sedimentation	2
2.1.2 Diffusion	2
2.1.3 Coalescence	3
2.1.4 Asphaltenes in Crude Oil	3
2.2 Types of Separators for Subsea Separation	4
2.2.1 Gravity Separation Vessels	4
2.2.2 Pipe Separators	4
2.2.3 In-Line Swirl Separators	5
2.2.4 Electrostatic Coalescer	5
2.3 Separation Models Based on Population Balances	6
3 Model Description	6
3.1 Horizontal Gravity Separator	6
3.2 Swirl Separator	10
4 Results	14
4.1 Gravity Separator	14
4.1.1 Impact of Characteristic Drop Size	17
4.2 Swirl Separator	18
4.2.1 Effect of the Flow Rate on Separation	19
4.3 Combined System	20
5 Conclusion	22
References	23
A MATLAB Code	24
A.1 Main Script	24
A.2 Separation System Function: separation.m	29
A.3 Swirl Separator Script	32
B Effect of Fluid Parameters on Separation	34
C Moody Diagram	35

List of Figures

1	Surfactants on droplet	3
2	Asphaltene distribution in separator	3
3	Pipe separator	4
4	Swirl element in swirl separator	5
5	Co-current and counter-current swirl separators	5
6	Horizontal gravity separator	6
7	Gravity separator at complete separation	7
8	Gravity separator with incomplete separation	7
9	Gravity separator in model	9
10	Modeled asphaltene distribution in gravity separator	9
11	Swirl separator	10
12	Approximations of tangential velocity in swirl separator	12
13	Inner pipe and oil core in swirl separator	13
14	Modeled asphaltene distribution in swirl separator	14
15	Gravity separator: +5 % step change in feed rate	16
16	Gravity separator: -5 % step change in feed rate	17
17	Swirl separator: Outlet composition vs. volumetric flow rate	19
18	Effect of angular velocity on degree of separation	20
19	Separation system with gravity- and swirl separator: PFD	21
20	Separation system with gravity- and swirl separator: Simulations	21
C.1	Moody Diagram	35

List of Tables

1	Physical properties of the emulsion in the gravity separator	15
2	Physical dimensions of the gravity separator	15
3	Nominal state of gravity separator	15
4	Impact of characteristic drop size on separation	18
5	Physical parameters of the swirl separator	18
6	Physical properties of the emulsion in the swirl separator	19
B.1	Impact of characteristic drop size on separation	34
B.2	Impact of density on separation	34
B.3	Impact of water viscosity (temperature) on separation	34

List of Symbols

Latin Letters

Symbol	Description	Unit
a_c	Centrifugal acceleration	m/s^2
C	Concentration	mol/m^3
C_{decay}	Decay factor for lost momentum	–
D	Diffusion coefficient	m^2/s
F_d	Drag force	N
F_g	Gravitational force	N
f_t	Fraction of \dot{q}_{us} to top outlet	–
g	Gravitational acceleration (≈ 9.81)	m/s^2
h	Hight of water phase	m
h_1	Hight of pure water	m
HPO	Abbreviation: Heavy Phase Outlet	–
k	Proportionality constant	m^{-3}
L_{sep}	Length of separator	m
L_1	Required length of separator for complete separation	m
LPO	Abbreviation: Light Phase Outlet	–
\dot{q}_b	Bottom outlet volumetric flow	m^3/s
\dot{q}_{HPO}	Volumetric flow in heavy phase outlet	m^3/s
\dot{q}_{in}	Inlet outlet volumetric flow	m^3/s
$\dot{q}_{i,j}$	Volumetric flow of component i in stream j	m^3/s
\dot{q}_{LPO}	Volumetric flow in light phase outlet	m^3/s
\dot{q}_m	Middle outlet volumetric flow	m^3/s
\dot{q}_t	Top outlet volumetric flow	m^3/s
\dot{q}_{us}	Volumetric flow of unseparated emulsion	m^3/s
\dot{q}'_{us}	Volumetric flow of unseparated emulsion to top- and bottom outlet	m^3/s
R	Radius of separator	m
R_c	Radius of core with solid body rotation $\approx 0.25R$	m
R_i	Radius of inner pipe in swirl separator	m
r	Radial dimension	m
r_{in}	Radial position at inlet	m
r_{out}	Radial position at outlet	m
r_d	Characteristic droplet radius	m
t	Time	s
t_a	Residence time of droplet in swirl separator	m
V_d	Droplet voulme	m^3
V_a	Total volume of asphaltenes in separator	m^3
V_{liq}	Total volume of liquid in separator	m^3
V_o	Total volume of oil phase in separator	m^3
V_{S1}	Total volume of oil-in-water emulsion	m^3
V_{S2}	Volume of oil-in-water emulsion that will get separated	m^3
V_{S1}	Volume of oil-in-water emulsion that is will not get separated	m^3
V_w	Total volume of water phase in separator	m^3
v	Velocity	m/s
v_a	Axial velocity of droplet	m/s
v_h	Horizontal velocity of droplet	m/s

Symbol	Description	Unit
v_r	Radial velocity of droplet	m/s
v_t	Angular velocity of droplet	m/s
v_v	Vertical velocity of droplet	m/s
wc	Water cut/Volume fraction of water in inlet stream	–
x	Horizontal dimension	m
$x_{a,i}$	Volume fraction of asphaltene in stream i	–
z	Vertical/axial dimension in gravity/swirl separator	m
z_b	Location of bottom outlet	m
z_m	Location of middle outlet	m
z_t	Location of top outlet	m

Greek Letters

Symbol	Description	Unit
α	Correlation factor for asphaltene solubility	–
ε	Volume fraction of unseparated emulsion	–
θ	Angle between oil-water interface and gravitational direction	rad
θ_1	Angle between pure water pure water and gravitational direction	rad
μ_w	Viscosity of water	$Pa \cdot s$
π	the ratio of a circle's circumference to its diameter	–
ρ	Density of continuous phase	kg/m^3
ρ_d	Droplet density	kg/m^3
ρ_o	Oil density	kg/m^3
ρ_w	Water density	kg/m^3
φ	Angle of longest droplet path for complete separation	rad
φ_1	Actual angle of longest droplet path	rad
ω	Angular frequency og swirl flow	rad/s
ω_0	Angular frequency of swirl flow just downstream of swirl element	rad/s

1 Introduction

There is an increasing demand for subsea separation in the oil and gas industry. Subsea separation allows fields with lower economic potential (e.g. lower reservoir pressures, deeper waters etc.) than earlier to be used or considered for oil production. The operating costs are reduced by avoiding the use of energy to pump the produced water to the surface and rather pump it back down into the reservoir or release it into the sea. Reduced operating costs prolong the period of time in which production is economically favorable and thus increase the recovery and economic potential of the field. The need for large platforms is also reduced and the oil from several smaller reservoirs can be separated on the seabed before being pumped up to one common topside facility (e.g. platform, FPSO).

With the benefits of subsea separation comes several challenges. The reduced accessibility leads to difficulties in maintenance and changing out equipment parts. The subsea separators also have stricter limitations when it comes to size compared to topside separators. The separators have to be lowered down to the seabed by ship cranes in moving, and sometimes deep, waters, which makes large processing units undesirable to use. The small sizes of the separators lead to control challenges due to short residence times and optimization becomes more vital because of the reluctance to oversize the equipment. In addition, changes in operating conditions during the lifetime of the field needs to be dealt with, which makes automation important.

To deal with the separation challenges, it is important to have a good model of the separation process. For control purposes, this model needs to be simple, but at the same time accurate. The objective for this project was to develop a model for a oil-water separation system that can be used for further work regarding optimization and control of these kind of systems.

2 Separation Theory

This section covers the basic physical principles behind the separation of emulsions and a short overview of some available compact separation units for subsea oil-water separation. In addition, a short introduction to how liquid-liquid separators can be modeled by the use of population balances is included.

2.1 Principles of Separation Theory

2.1.1 Sedimentation

When the dispersed liquid in an emulsion has a density that differs from the density of the continuous phase, it will sediment or cream due to gravitational forces. A droplet with density ρ_d and volume V_d in a medium with density ρ will be exposed to the gravitational force [6];

$$F_g = V_d(\rho_d - \rho)g \quad (2.1)$$

where g is the gravitational acceleration which can be replaced by a greater value if the driving force is something else than gravity (e.g. swirl separators). The frictional force, F_d , on a small sphere moving through a viscous fluid can be expressed by Stoke's law [6];

$$F_d = 6\pi\mu r_d v \quad (2.2)$$

where μ is the viscosity of the continuous phase, r_d is the radius of the droplet and v is the velocity of the droplet. By combining equation 2.1 and 2.2 the terminal velocity of a single droplet relative to the medium can be expressed as:

$$v = \frac{2r_d^2(\rho_d - \rho)g}{9\mu} \quad (2.3)$$

The assumption for Stoke's law is relatively robust for small volume fractions, ϕ_0 , of the dispersed fluid, but at higher volume fractions, the interactions between each droplet will become more dominant and the terminal velocity will be reduced. This can be compensated for by multiplying the right hand side of equation 2.3 by a correction factor, $F(\phi_0)$. A theoretical calculation of this factor is very complicated, but relatively good estimations can be found experimentally [6] for a given system.

2.1.2 Diffusion

As soon as the separation process starts due to sedimentation there will arise concentration gradients in the direction of separation. This again will lead to diffusion by Brownian motions which will have an opposing effect on the separation. The diffusion in an emulsion with a concentration difference in the x-direction can be expressed by Fick's 2. law;

$$\frac{dC(t, x)}{dt} = D \frac{\partial^2 C(t, x)}{\partial x^2} \quad (2.4)$$

where D is the diffusion constant for the given system and $C(t, x)$ is the concentration of the dispersed phase.

2.1.3 Coalescence

Different droplets will have different velocities caused by sedimentation (i.e. they have different sizes) and diffusion. This again leads to collisions which may cause them to coalesce dependent on the kinetic energy of the droplets and the attractive and repulsive forces between them. The coalescence rate will therefore depend of the nature of the two phases and will decrease significantly by the presence of surfactants (see section 2.1.4).

It is possible to derive a theoretical expression for the coalescence efficiency [4] for a given system. This does, however, depend on the interfacial tension of the emulsion which gets quite complicated for a crude oil-water emulsion as the crude oil composition varies from one system to another.

2.1.4 Asphaltenes in Crude Oil

Asphaltenes are defined as the fraction of a crude oil that is soluble in toluene and insoluble in heptane [14]. The insolubility in alkanes will cause the asphaltenes to act as surfactants in water-oil emulsions, Figure 1, which lowers the interfacial tension and leads to a reduced coalescence rate. The time required to separate an oil-water emulsion will therefore depend on the concentration of asphaltenes in the crude oil.

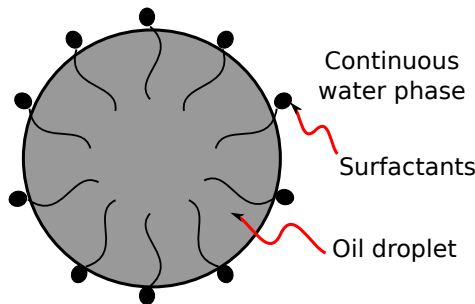


Figure 1: Surfactants on an oil droplet in a continuous water phase

The asphaltene concentration in a separator will increase with the droplet concentration, i.e. it will peak at the interface between the continuous oil and continuous water phase as illustrated in Figure 2. This may lead to accumulation of asphaltenes in the separator as the out flows are located at the top and bottom of the separator. This is an undesirable behavior as it leads to reduced separation.

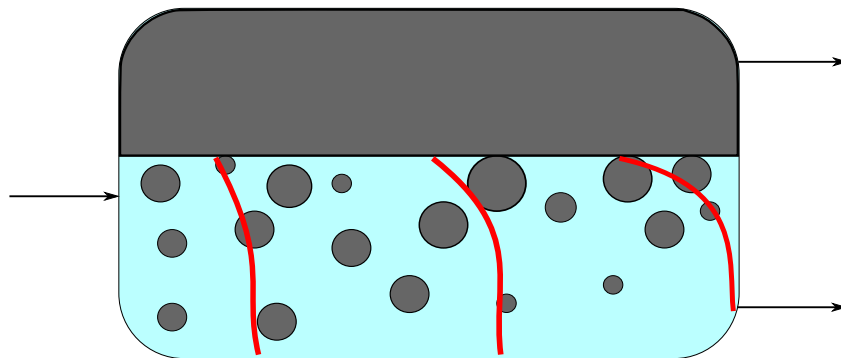


Figure 2: Gravity separator with a oil-in-water emulsion. The red curves represent the qualitative surfactant concentration through the separator.

2.2 Types of Separators for Subsea Separation

Many types of separators can be used for subsea oil-water separation. Normally there are several units combined to maximize the degree of separation. This section is meant to give a short introduction to some of the different types of separators and the pros and cons of each alternative.

2.2.1 Gravity Separation Vessels

Traditional gravity separators require large volumes compared to the other alternatives for a given separation quality. They are therefore not very suitable for doing a large share of the separation in a subsea separation systems. They are, however, robust and can handle large amounts of gas together with oil and water. A possible usage of gravity separators subsea, is letting it do the bulk separation and then use more advanced alternatives to remove the remaining impurities of the outlet streams.

A second alternative is to have another type of separator (e.g. a pipe separator, see section 2.2.2) do the majority of the separation first and then use the gravity separator to complete the separation. A possible reason for doing this is that you cannot have level control directly on a pipe separator and it therefore becomes difficult to split the oil from the water even if you have two separate phases. This application of a gravity separator is used for the SSAO Marlim Project [7].

2.2.2 Pipe Separators

Pipe separators do gravity driven separation of oil and water. They differ from traditional gravity separators in that they are much longer and thinner. This results in shorter distances for each droplet to travel in that the interface between the bulk phases is closer to the pipe wall and thus the separation rate is significantly increased. The small pipe diameter also lead to an increased relative interfacial area between the bulk phases for the droplets to pass through [3].

Pipe separators can have turns like the illustration in Figure 3. This leads to a centrifugal force being introduced in parts of the separator which again leads to an increased separation rate in these regions.



Figure 3: Pipe separator with two turns with radius R_1 and R_2 resulting in centrifugal forces being introduced.

The short diameters of the pipe separators result in higher Reynolds numbers and a greater tendencies to turbulent flow. Increased turbulence counteracts separation and can therefore be a problem for pipe separators. It is thus critical to keep the gas content as low as possible , e.g. have a gas/liquid separator upstream of the separation pipe.

2.2.3 In-Line Swirl Separators

There exists many types of separators using centrifugal forces as the main driving force. Centrifugal forces can be introduced by external work, the flow entering tangential on an arched wall or with a static swirl element in the pipe. In-line swirl separator use the latter technology. The flow enters the separator and passes a static swirl element equipped with vanes that deflect the flow so it gets a swirling flow pattern [9] as illustrated in Figure 4. The centrifugal force introduced can easily be a hundred times larger than gravity [9] and will therefore increase the separation rate significantly.



Figure 4: Swirl element. The flow enters the separator and a static swirl element introduces an angular velocity causing the fluid to have a swirling flow through the separator.

In-line swirl separators can be divided into two main categories. Counter-current swirl separators [1, 13] have the light- and heavy phase exiting in the opposite directions, while co-current swirl separator [11, 9] have both phases exiting in the same direction. This is illustrated in Figure 5.

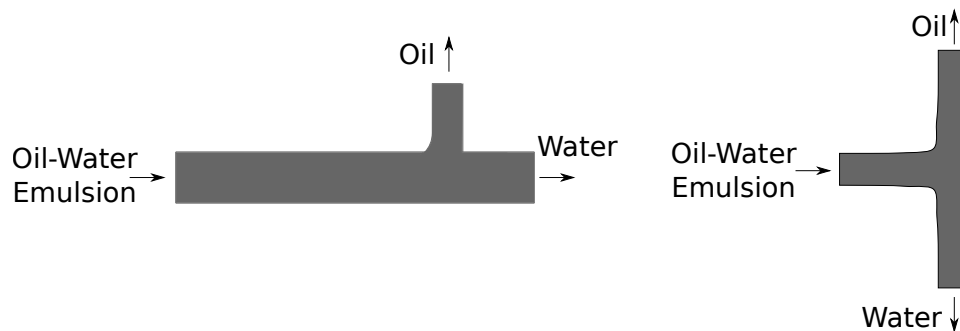


Figure 5: In-Line Swirl Separators. **Left:** Co-current. **Right:** Counter-current.

2.2.4 Electrostatic Coalescer

Electrostatic coalescers are used to increase the size of the water droplets in a continuous oil phase and are typically applied on the oil outlet of upstream separation units to treat the remaining water. There is an electrostatic field across the unit, which causes the the water droplets to coalesce by migration and dipolar coalescence [10]. Migration is a process where charged droplets are pulled by the applied electric field causing them to colloid. The droplets can possess electric charges due to preferential adsorption or contact with the electrodes. Dipolar coalescence takes place as a result of the droplets being polarized by the electric field. This gives rise to attractive forces between them which pull them together and hence increase the coalescence rate. These coalescence principles requires a dielectric continuous phase and a polar dispersed phase, which means it can only be applied for emulsions where the oil is the continuous phase.

The electrostatic coalescer increases the droplet size which makes further separation much easier. It is typically the smallest droplets that remain unseparated after the initial separation and in order to achieve very low water concentrations without using enormous volumes, a electrostatic coalescer might be necessary. The coalescer will typically be placed

upstream of a gravity separator that separates the enlarged water droplets out of the emulsion [2].

2.3 Separation Models Based on Population Balances

The principles of separation described in section 2.1 can be combined to make a model for any given separator. Most real emulsions are polydisperse (i.e. they have non-uniform drop size distributions) which leads to different sedimentation velocities and affects the diffusion and coalescence. The drop size distribution will change during the residence time in the separator due to coalescence and this again makes it necessary to use a population balance in order to get an accurate model.

A model based on a population balance for water-oil separation in a gravity driven, batch separator has been developed by Grimes, B. [4]. The model requires the basic physical parameters of the emulsion (e.g. densities, viscosity etc.), the interfacial tension, the physical dimensions of the separator and the initial drop size distribution of the dispersed phase. In addition, it has four tuning parameters that can be used to fit the model to experimental data. The model shows good agreement with experimental data even with minimum use of the fitting parameters [5]. The simulation time is, however, 6-10 hours and it is reasonable to believe that this time will increase for more complicated systems (e.g. continuous processes, swirl flow etc.). It is therefore desirable to have a simplified model for these kinds of separation systems.

3 Model Description

This section describes models for a gravity and a co-current swirl separator by the use of characteristic drop sizes. These models are significantly simplified compared to models based on populations balances. This reduces the accuracy of the models, but may be useful for applications where lower simulation times are desirable.

3.1 Horizontal Gravity Separator

The model for the horizontal gravity separator is based on the method described by Sayda and Taylor [8]. It is assumed that the inlet flow is a continuous water phase with oil droplets and that the flow pattern is plug flow through the separator. The oil droplets move upwards and join the continuous oil phase before exiting through the top outlet and the purified water exits through the bottom outlet, see Figure 6. There is left an empty space in the upper part of the separator where a gas-model and a gas outlet can be added if desirable. Or, the oil level can be set as the total height of the separator if there is no gas content in the incoming flow.

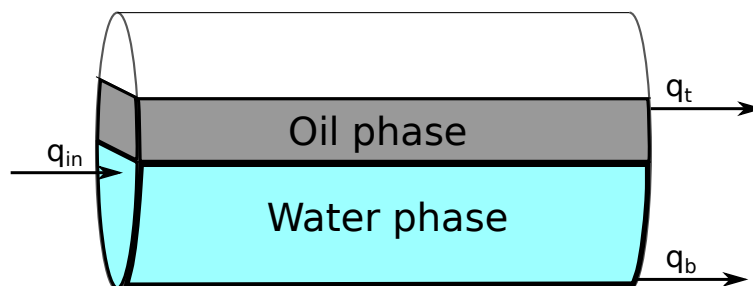


Figure 6: Horizontal gravity separator

The horizontal velocity of the oil droplets, v_h , is assumed to be equal to the surrounding water phase and can be described by;

$$v_h = \frac{\dot{q}_b L_{sep}}{V_w} \quad (3.1)$$

where V_w is the volume of the water phase, \dot{q}_b is the volumetric flow rate of the bottom outlet and L_{sep} is the length of the separator. The vertical velocity, v_v , is assumed to follow Stokes' law as described in section 2.1.1, hence it is given by;

$$v_v = \frac{2g(\rho_o - \rho_w)r_d^2}{9\mu_w} \quad (3.2)$$

where g is the gravitational acceleration ($\approx -9.8 \text{ m/s}^2$), ρ_o and ρ_w are the densities of the oil and water phase, μ_w is the viscosity of water and r_d is the characteristic droplet radius.

Complete separation occurs as long as the vertical velocity is sufficiently large compared to the horizontal velocity, see Figure 7. The angle, φ , of the longest droplet path to the oil-water interface is defined as:

$$\varphi = \arctan\left(\frac{v_v}{v_h}\right) \quad (3.3)$$

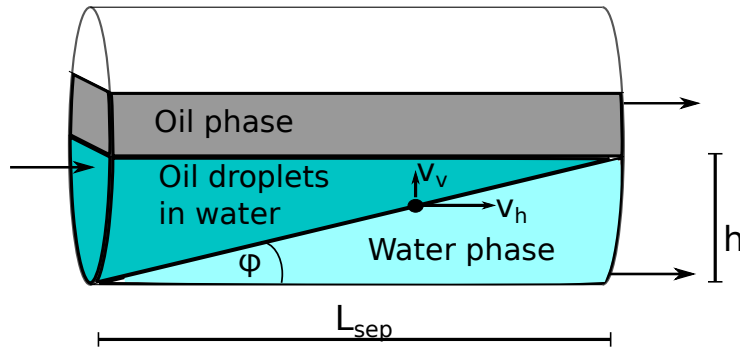


Figure 7: Horizontal gravity separator with complete separation. The diagonal line between the pure water and oil-in-water emulsion represent the longest distance an oil droplet has to travel to the oil interface.

If the volumetric flow rate is increased from the situation in Figure 7, some of the oil will still be unseparated when it reaches the end of the separator. By doing a hypothetical extension of the separator, complete separation would occur at a length $L_1 > L_{sep}$ as illustrated in Figure 8.

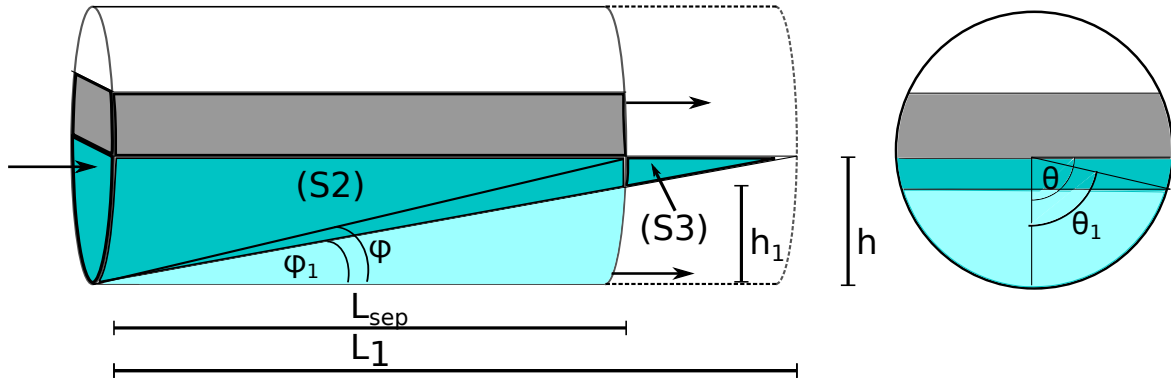


Figure 8: Left: Horizontal gravity separator with incomplete separation. The three sections are pure oil/ oil-in-water emulsion/ pure water as in Figure 7. Right: Cross section of the separator at the length L_{sep} .

The section with oil-in-water emulsion i Figure 8 is represented by $S1 = S2 + S3$. The volume of this section is given by the difference between the cylinder segment defined by R , L_1 and h and the cylindrical wedge defined by R , L_1 and φ_1 . The volume of section $S1$ can be expressed as;

$$V_{S1} = R^2 L_1 \left[\theta - 0.5 \sin(2\theta) - \frac{3 \sin(\theta) - 3\theta \cos(\theta) - \sin^3(\theta)}{3(1 - \cos(\theta))} \right] \quad (3.4)$$

where R is the radius of the separator and L_1 , θ (equation 3.6) and φ_1 (equation 3.3) are defined in Figure 8. Similarly, the volume of section $S2$, V_{S2} , is the difference between the cylinder segment given by R , L and h and the cylindrical wedge given by R , L and φ_1 .

$$V_{S2} = R^2 L_{sep} \left[\theta - 0.5 \sin(2\theta) - \frac{3 \sin(\theta_1) - 3\theta_1 \cos(\theta_1) - \sin^3(\theta_1)}{3(1 - \cos(\theta_1))} \right] \quad (3.5)$$

The angles, θ and θ_1 are defined by;

$$\theta_i = \arccos \left[1 - \frac{h_i}{R} \right] \quad (3.6)$$

and L_1 and h_1 are given by:

$$h_1 = L_{sep} \tan(\varphi_1) \quad (3.7)$$

$$L_1 = \frac{h}{\tan(\varphi_1)} \quad (3.8)$$

The volume of the unseparated emulsion $V_{S3} = V_{S1} - V_{S2}$. This leads to an explicit expression for the volume fraction of the unseparated emulsion, ε , as shown i equation 3.9. Hence, the flow rate of oil droplets crossing the oil-water interface, \dot{q}_s , (i.e. the separation rate) is defined in equation 3.10.

$$\varepsilon = \begin{cases} 1 - \frac{V_{S2}}{V_{S1}}, & L_1 > L_{sep} \\ 0, & L_1 \leq L_{sep} \end{cases} \quad (3.9)$$

$$\dot{q}_s = (1 - \varepsilon) \dot{q}_{o,in} = (1 - \varepsilon)(1 - wc) \dot{q}_{in} \quad (3.10)$$

Where $\dot{q}_{o,in}$ is the inlet flow of oil and wc is the water volume fraction of the inlet flow. The unseparated emulsion at the end of the separator has a volumetric flow, \dot{q}_{us} defined in equation 3.11 and a water volume fraction equal to the one in the inlet flow. This flow will undergo turbulence at the end of the separator and exit through the outlets as illustrated in Figure 9. If the bottom outlet is located at the hight z_b and the top outlet at z_t , the fraction of \dot{q}_{us} exiting through the top outlet, f_t , is assumed to be given by equation 3.12. The quality of this assumption depends on the geometry and structure of the outlets, but it gives a reasonable estimation of the composition of the out flows as a function of the level of the oil-water interface, h .

$$\dot{q}_{us} = \varepsilon \dot{q}_{in} \quad (3.11)$$

$$f_t = \frac{h_1 - z_b}{(z_t - h) + (h_1 - z_b)} \quad (3.12)$$

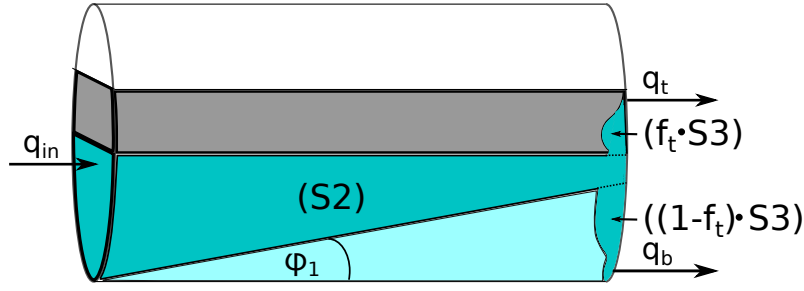


Figure 9: Horizontal gravity separator with incomplete separation. The three sections are pure oil/ oil-in-water emulsion/ pure water as in Figure 7.

It is assumed that the asphaltene concentration increases linearly from the bottom of the separator to the oil-water interphase due to the increasing amount of droplets (see section 2.1.4). It is also assumed that a given fraction, α , of the asphaltenes will go into the continuous oil phase. Hence, the volume fraction of asphaltenes in the oil, $x_{a,o}$, and water, $x_{a,w}$ are defined by equation 3.13 and 3.14 as illustrated in Figure 10.

$$x_{a,o} = \alpha \frac{V_a}{V_{liq}} \quad (3.13)$$

$$x_{a,w}(z) = (1 - \alpha) a \frac{z}{h} \frac{V_a}{V_{liq}} \quad (3.14)$$

Where V_a is the total volume of asphaltenes in the separator, V_{liq} is the total liquid volume and h is the height of the water phase. The constant a scales the expression so the average volume fraction of asphaltene in the water phase is $(1 - \alpha)V_a/V_w$. If $h \approx R$, then $a \approx 3$. The asphaltene model is included in order to make it possible to track the asphaltenes through a separation system. It is, however, not very accurate and should be improved for further work with the model.

An optional, third outlet stream, \dot{q}_m , is included in order to make it possible to control the surfactant concentration in the separator. See Figure 10. For this stream to have any effect, it is essential that the oil-water interface is located close to the middle outlet.

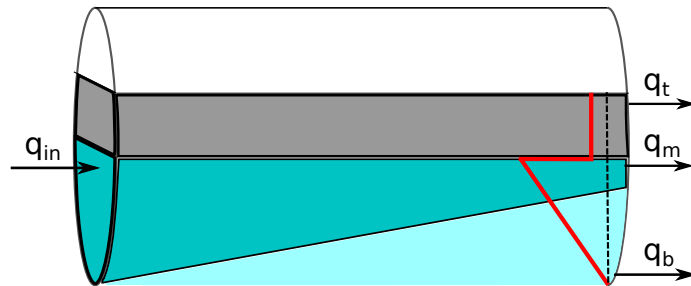


Figure 10: The red curve represent the asphaltene concentration as function of the height at the end of the separator. The three sections are pure oil/ oil-in-water emulsion/ pure water as in Figure 7.

If the unseparated liquid flow, \dot{q}_{us} , is large than the third outlet flow, \dot{q}_m , the unseparated flow going out of the top and bottom outlet, \dot{q}'_{us} will be defined as:

$$\dot{q}'_{us} = \dot{q}_{us} - \dot{q}_m \quad (3.15)$$

The mass balance for the continuous water phase can then be formulated as the volumetric balance in equation 3.16. The assumption made here implies that the density of the inlet flow is equal to the density of the combined outlet flows. Note that this is not a component balance, but a balance for the entire water phase, including the dispersed oil droplets.

$$\frac{dV_w}{dt} = \dot{q}_{in} - \dot{q}_s - f_t \dot{q}'_{us} - \dot{q}_m - \dot{q}_b \quad (3.16)$$

Where V_w is the volume of the water phase, \dot{q}_{in} is the total inlet flow rate, \dot{q}_s is the separation rate (equation 3.10), \dot{q}'_{us} is the unseparated flow rate (equation 3.15) of which the fraction f_t (equation 3.12) exits through the top outlet and \dot{q}_m and \dot{q}_b are the flow rates out of the separator through the middle and bottom outlet, respectively.

Similarly, the volumetric balance of the continuous oil phase can then be expressed as;

$$\frac{dV_o}{dt} = \dot{q}_s - [\dot{q}_t - f_t \dot{q}'_{us}] \quad (3.17)$$

where V_o is the volume of the continuous oil phase and \dot{q}_t is the flow rate through the top outlet.

3.2 Swirl Separator

The model for the co-current, in-line swirl separator is based on similar principles as the gravity separator. The main difference is that the gravitational force is replaced by a centrifugal force caused by the swirling flow. The model is described for oil droplets in a continuous water phase, but only small changes are needed for the opposite situation (i.e. water-in-oil emulsion).

The inlet stream passes the swirl element and flows through the separator with a swirling flow pattern. The density difference between the oil droplets and the continuous water phase causes the droplets to be pushed in towards the center of the separator. See Figure 11. At the end of the separator there is light phase outlet (LPO) with radius $R_i < R$ where the inner fraction of the flow is extracted while the the liquid outside of this radius continues and exits through the heavy phase outlet (HPO).

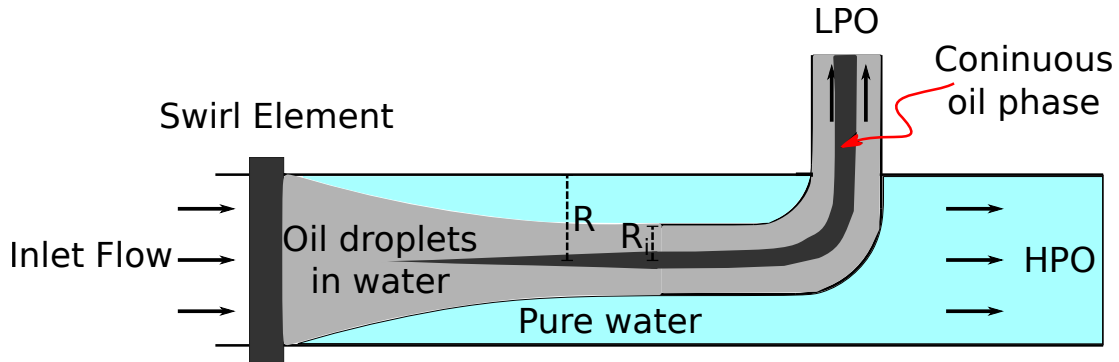


Figure 11: The inlet flow is separated by centrifugal forces to the light phase outlet (LPO) and heavy phase outlet (HPO).

The droplets are assumed to have an axial velocity equal to that of the surrounding continuous phase and the axial flow pattern is assumed to be plug flow. The axial velocity,

v_a , of any droplet in the separator is then defined as;

$$v_a = \frac{\dot{q}_{in}}{\pi R^2} \quad (3.18)$$

where \dot{q}_{in} is the inlet flow rate and R is the radius of the separator. The residence time of the droplets in the separator, t_a , is given by;

$$t_a = \frac{L}{v_a} \quad (3.19)$$

where L is the length of the separator. The radial velocity, $v_r(r)$, of any droplet can be found by replacing the gravitational acceleration, g , in equation 2.3 with the centrifugal acceleration a_c . It is assumed that $a_c \gg g$ so that the gravitational acceleration can be neglected. The radial velocity is then given by;

$$v_r(r) = \frac{2(\rho_o - \rho_w)r_d^2 a_c(r)}{9\mu_w} \quad (3.20)$$

where r is the distance from the droplet to the center of the separator, ρ_o and ρ_w are the densities of the oil and water, μ_w is the viscosity of water and r_d is the characteristic droplet radius. The centrifugal acceleration is defined as;

$$a_c(r) = \frac{v_t(r)^2}{r} \quad (3.21)$$

where v_t is the tangential velocity of the fluid. The initial assumption is that the swirl flow has a solid body rotation which means that the angular frequency ω is independent of the radial position, r . It is also assumed that the angular frequency just downstream of the swirl element, ω_0 , is proportional to the axial velocity at the swirl element and therefore also the volumetric flow, as stated in equation 3.22. This implies that the drag force is assumed to be proportional to the velocity of the liquid. This assumption should be robust when the Reynolds number is low, but can get inaccurate if the Reynolds number is too high.

$$\omega_0(\dot{q}_{in}) = k\dot{q}_{in} \quad (3.22)$$

Where k is a constant determined by the geometry of the swirl element. It is reasonable to assume that the angular frequency will decay down the separator. Slot [9] has modeled the angular frequency, $\omega(z)$, as a function of axial position as in equation 3.23. For this work, however, the decaying factor, C_{decay} , is neglected. The angular frequency is then independent of the axial position as in equation 3.24.

$$\omega(z) = \omega_0 e^{-C_{decay}z/2R} \quad (3.23)$$

$$\omega(z) \approx \omega_0 \quad (3.24)$$

Where z is the axial coordinate.

The initial assumption of the tangential velocity was that the entire swirl flow had a solid body rotation. However, the drag force from the pipe wall causes the tangential velocity of a swirling pipe flow to have a distribution similar to that of the Rankine vortex [9], see Figure 12. The initial assumption can then be improved by dividing the tangential velocity into two regions;

$$v_t(r) = \begin{cases} 2\pi r\omega, & 0 \leq r < R_c \\ 2\pi R_c\omega, & R_c \leq r \leq R \end{cases} \quad (3.25)$$

where R_c is the radius of an imagined core with solid body rotation. Experimental data for oil-in-water emulsions give a rough estimate for $R_c \approx 0.25R$ [9].

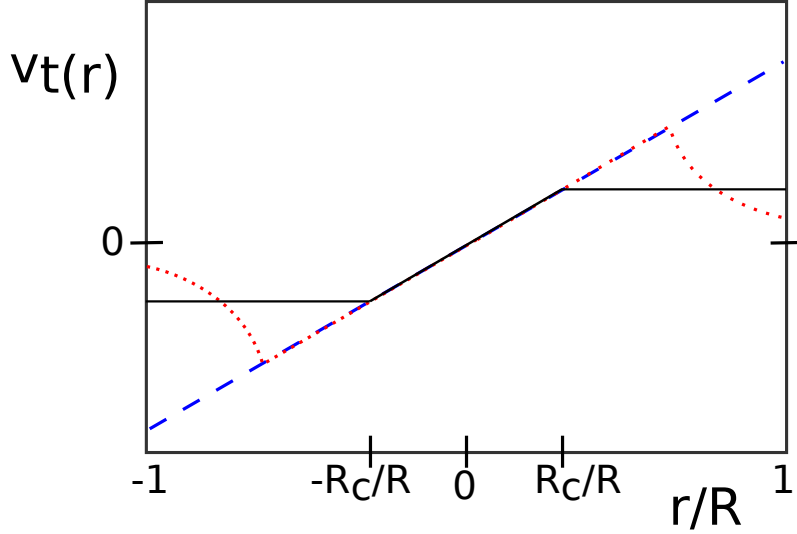


Figure 12: Tangential velocity , v_t , as a function of radial position r in a swirl separator with radius R . Solid line: Used approximation, Dashed line: No drag from wall, Dotted line: Rankine vortex.

Considering a droplet entering the separator at the radial position $r = r_{in}$ and axial position $z = 0$ and exiting the separator at $r = r_{end}$ and $z = L$. By setting the axial residence time, t_a equal to the radial residence time, t_r , this can be written as:

$$\int_{r_{in}}^{r_{end}} \frac{dr}{v_r(r)} = \int_0^{t_a} dt \quad (3.26)$$

If $r_{in} > R_c$ and $r_{end} < R_c$ it can be rewritten as:

$$\int_{r_{in}}^{R_c} \frac{dr}{v_r(r)} + \int_{R_c}^{r_{end}} \frac{dr}{v_r(R_c)} = t_a \quad (3.27)$$

An explicit expression for r_{in} can be derived by combining equation 3.27 with equation 3.20, 3.21 and 3.25:

$$r_{in}(r_{end}) = R_c \exp\left(-\frac{2(\rho_o - \rho_w)r_d^2}{9\mu_w}(2\pi\omega)^2 t_a + \frac{r_{end}^2 - R_c^2}{2R_c^2}\right) \quad (3.28)$$

If the axial flow pattern is plug flow, the flow rates out of the separator are simply functions of the radius of the inner- and outer pipe;

$$\dot{q}_{LPO} = \left(\frac{R_i}{R}\right)^2 \dot{q}_{in} \quad (3.29)$$

$$\dot{q}_{HPO} = \left(1 - \left(\frac{R_i}{R}\right)^2\right) \dot{q}_{in} \quad (3.30)$$

where \dot{q}_{LPO} and \dot{q}_{HPO} are the volumetric flow rates at the light- and heavy phase outlet, respectively. R_i and R are the radius of the inner- and outer pipe, while \dot{q}_{in} is the volumetric

flow rate at the inlet of the separator. The variables are shown in Figure 11.

If $r_{end} = R_i$ in equation 3.28, all the droplets that were inside of the radius r_{in} at the inlet, will be inside of the radius R_i at the end of the separator and thus be located in the LPO. This is, however, only valid if the cylindrical continuous oil phase that is formed in the center of separator has a smaller radius than the inner pipe. When the the continuous oil phase is wider than the inner pipe, the redundant oil will exit through the heavy phase outlet. The two situations are illustrated in Figure 13.

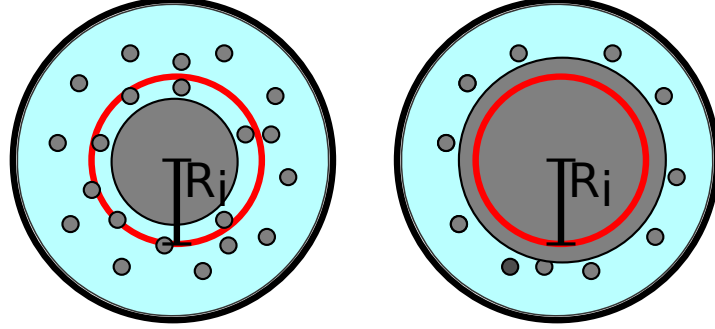


Figure 13: Cross section of the pipe separator at $z=L$. The separated oil droplets have formed a continuous oil phase (grey) in the middle of the separator. The inner pipe (red) has a radius R_i . **Left:** The radius of the inner pipe is sufficiently large compared to the continuous oil phase so that all the separated oil exits through the LPO. **Right:** The radius of the inner pipe is too small compared to the continuous oil phase, resulting in some of the separated oil exiting through the HPO.

It is assumed that the volume fraction of oil is homogeneously distributed at the inlet of the separator, $z = 0$. By setting $r_{end} = R_i$ in equation 3.28, the volumetric flow rate of oil, $\dot{q}_{o,LPO}$, in the LPO can be expressed as;

$$\dot{q}_{o,LPO} = \begin{cases} \left[\frac{r_{in}(R_i)}{R} \right]^2 (1 - wc) \dot{q}_{in}, & \left[\frac{r_{in}(R_i)}{R} \right]^2 (1 - wc) \dot{q}_{in} < \dot{q}_{LPO} - \dot{q}_{a,LPO} \\ \dot{q}_{LPO} - \dot{q}_{a,LPO}, & \text{else} \end{cases} \quad (3.31)$$

where $\dot{q}_{a,LPO}$ is the volumetric flow rate of asphaltenes in the light phase outlet.

A very simple model for the asphaltene distribution has also been implemented. It is assumed that the concentration of asphaltenes decreases linearly with the radius and reaches zero at the pipe wall as shown in Figure 14. The volume fraction of asphaltenes at the outlet $x_{a,end}(r)$ is therefore given by;

$$x_{a,end}(r) = 3x_{a,in} \left(1 - \frac{r}{R} \right) \quad (3.32)$$

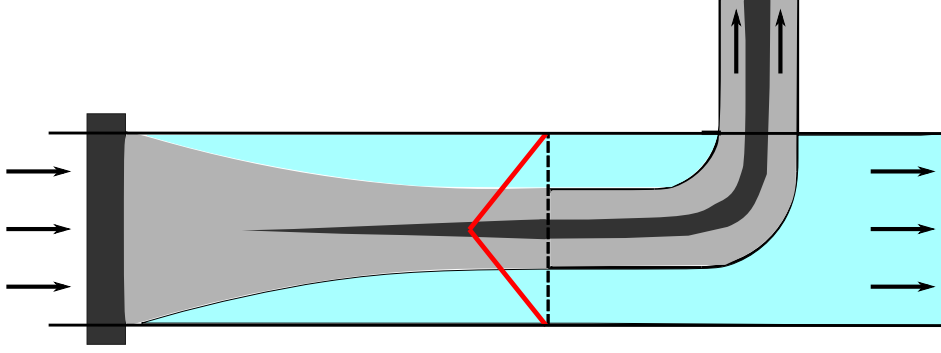


Figure 14: The red curve represent the asphaltene concentration as a function of the radial position in the separator at the length $z = L$.

The volumetric flow rate of each of the three components can now be defined for both outlets. The volumetric flow rates of asphaltenes $\dot{q}_{a,LPO}$ and $\dot{q}_{a,HPO}$ are derived by integrating the volume fraction in equation 3.32 and are given in 3.33 and 3.34, respectively.

$$\dot{q}_{a,LPO} = x_{a,in} \left[3 - 2 \frac{R_i}{R} \right] \dot{q}_{LPO} \quad (3.33)$$

$$\dot{q}_{a,HPO} = x_{a,in} \dot{q}_{in} - \dot{q}_{a,LPO} \quad (3.34)$$

The volumetric flow rate of oil exiting through the LPO is already defined in equation 3.31. The redundant oil, $\dot{q}_{o,HPO}$, will exit with the heavy phase and is defined by:

$$\dot{q}_{o,HPO} = (1 - wc - x_{a,in}) \dot{q}_{in} - \dot{q}_{o,LPO} \quad (3.35)$$

The water exiting through the light-, $\dot{q}_{w,LPO}$, and heavy phase outlet, $\dot{q}_{w,HPO}$, is simply defined as the difference between the total flow rates and the flow rates of oil and asphaltenes:

$$\dot{q}_{w,LPO} = \dot{q}_{LPO} - \dot{q}_{o,LPO} - \dot{q}_{a,LPO} \quad (3.36)$$

$$\dot{q}_{w,HPO} = \dot{q}_{HPO} - \dot{q}_{o,HPO} - \dot{q}_{a,HPO} \quad (3.37)$$

It is worth noting that unless the ratio $\left(\frac{R_i}{R}\right)^2$ is equal to the oil/water ratio in the inlet flow, you will reach a maximum value for the purity of either the LPO or the HPO even at complete separation. This problem can, however, be fixed by manipulating the ratio between the two outlet flows by introducing a pump or a valve on one of the outlet flows.

4 Results

This section is meant to give an overview of how the modeled separation performance is affected by different disturbances. Both models are discussed separately and in a combined system. The models are described in section 3 and the corresponding Matlab codes are given in Appendix A.

4.1 Gravity Separator

The performance of the separator is highly dependent on the nature (e.g. densities, viscosities, interfacial tension etc.) of the incoming fluid. There are also a significant variations in the physical properties of reservoir fluids for different oil fields and several

parameters must be known or assumed in order to do a simulation. The parameters in Table 1 are used in the simulations performed for this work and is meant to represent a typical crude oil-water emulsion from an oil field. The characteristic droplet size is the value that has the most influence on the performance of the separator. Typical initial droplet radiuses for crude oil-in-water emulsions are found in literature to be in the magnitude of $25 \mu m$ [9, 13]. The characteristic droplet radius is a parameter that gives a good estimation of the separation rate and will be greater than the average initial droplet radius due to coalescence of droplets in the separator. The characteristic droplet radius used for the simulations in this work is set to $250 \mu m$, which is also used for similar simulations performed by Sayda et al. [8]. This value might be high compared to a typical system and will therefore lead to low residence times required for good separation. The impact of changing the characteristic drop sizes is discussed further in section 4.1.1.

Table 1: Physical properties of the emulsion in the gravity separator

Symbol	Description	Value	Unit
r_d	Characteristic droplet radius	250	μm
ρ_o	Oil density	900	kg/m^3
ρ_w	Water density	1000	kg/m^3
μ_w	Viscosity of water (60 °C)	0.467	$mPa \cdot s$
$x_{a,in}$	Volume fraction of asphaltene in crude oil	0.025	–
wc	Volumetric water cut	0.5	–
α	In equation 3.13 & 3.14	0.1	–

The physical dimensions of the separator are listed in Table 2.

Table 2: Physical dimensions of the gravity separator

Symbol	Description	Value	Unit
R	Radius of separator	0.75	m
L_{sep}	Length of separator	4.6	m
z_t	Top outlet location	1.3	m
z_m	Middle outlet location	1.0	m
z_b	Bottom outlet location	0	m

The system was simulated with the nominal state described in Table 3. The levels of the two phases was controlled by PI-controllers paired with the top and bottom out flows to make the system stable. The flow rate of the middle outlet is set manually, but have been changed by the same factor as the feed rate for the simulations described below (i.e. manual ratio control).

Table 3: Nominal state of gravity separator

Symbol	Description	Value	Unit
\dot{q}_{in}	Feed rate	0.47	m^3/s
\dot{q}_t	Top outlet volumetric flow rate	0.24	m^3/s
\dot{q}_m	Middle outlet volumetric flow rate	0.01	m^3/s
\dot{q}_b	Bottom outlet volumetric flow rate	0.22	m^3/s
h	Water phase hight	1	m
h_2	Hight of total liquid	1.4	m

A 5 % step change in the feed rate (and middle outlet flow rate) was introduced at the time $t = 10$ s. The modeled impurities of the outlet flows are shown in Figure 15. As expected, the impurities of top and bottom outlet increases with the increased feed rate. This is caused by the increased horizontal velocity of the droplets, while the vertical velocity (i.e. sedimentation velocity) is unchanged. The water content of the middle outlet stream is unchanged. That is a consequence of the model regarding the unseparated section of the water phase, referred to as $S1$ in section 4.1, as a homogenous emulsion and does not consider accumulation of droplets on the oil-water interface. The real behavior may therefore differ from the simulated response shown in Figure 15.

There is a rapid change in the asphaltene content of the top- and bottom outlet. The increased flow rate causes the droplets near the interface to be pushed out through the outlets and with them comes the asphaltenes that are adsorbed on the interfaces. This causes the total amount of asphaltenes in the separator to be reduced, which again leads to less asphaltenes solved in the oil phase and the system slowly approaches a new steady-state. The modeled behavior of the asphaltenes is greatly simplified, but the response seems to agree with the initial idea about asphaltene accumulation in the separator for high degrees of separation.

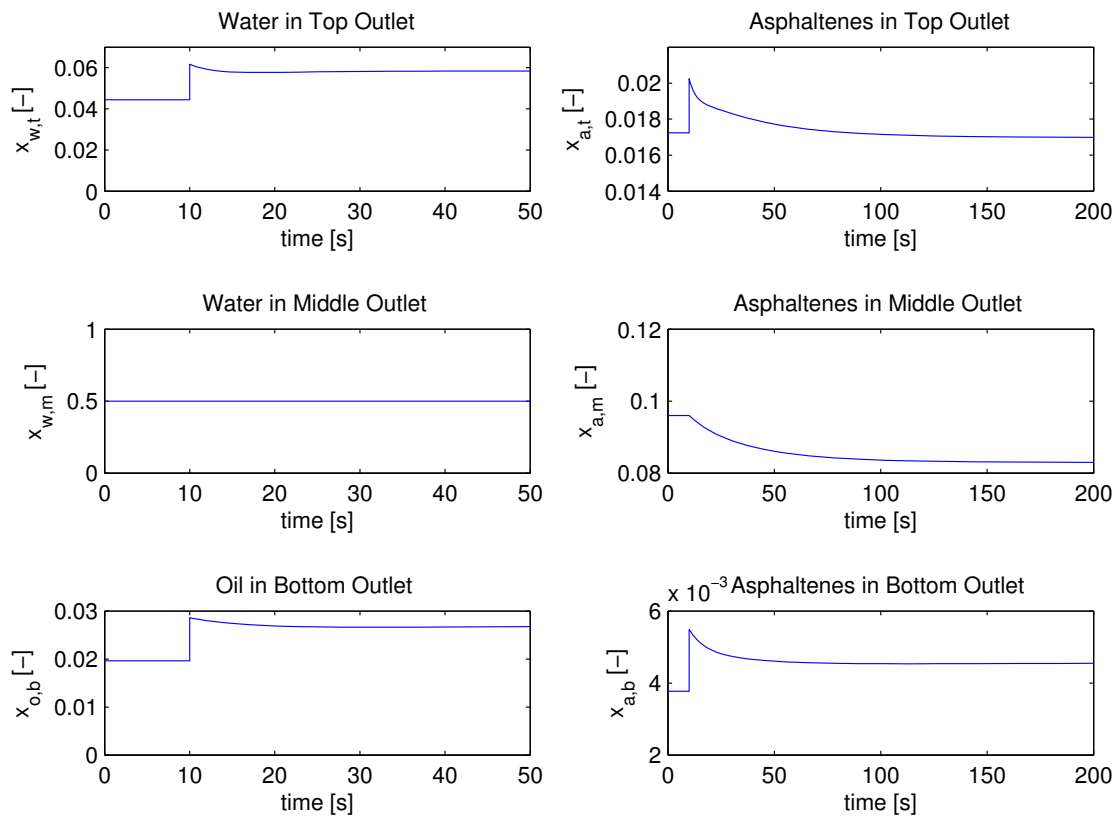


Figure 15: Simulated response of a 5 % increase in feed rate. The left hand side are the water and oil impurities of the outlet streams. The right hand side show the asphaltene content of each outlet stream.

Another simulation was performed by doing a 5 % reduction in the feed rate. The degree of separation is improved, see Figure 16, due to the increased residence time of the droplets.

The improved separation leads to an increased asphaltene content near the oil-water interface as can be seen from the composition of the middle outlet flow. The asphaltenes will in reality increase the stability of the emulsion and hence reduce the separation rate. The stabilizing effect of the asphaltenes is neglected in the model and this may lead to an overestimation of the degree of separation. In order to get an accurate model for this phenomena, experiments on the effect of asphaltenes on the separation rate is required.

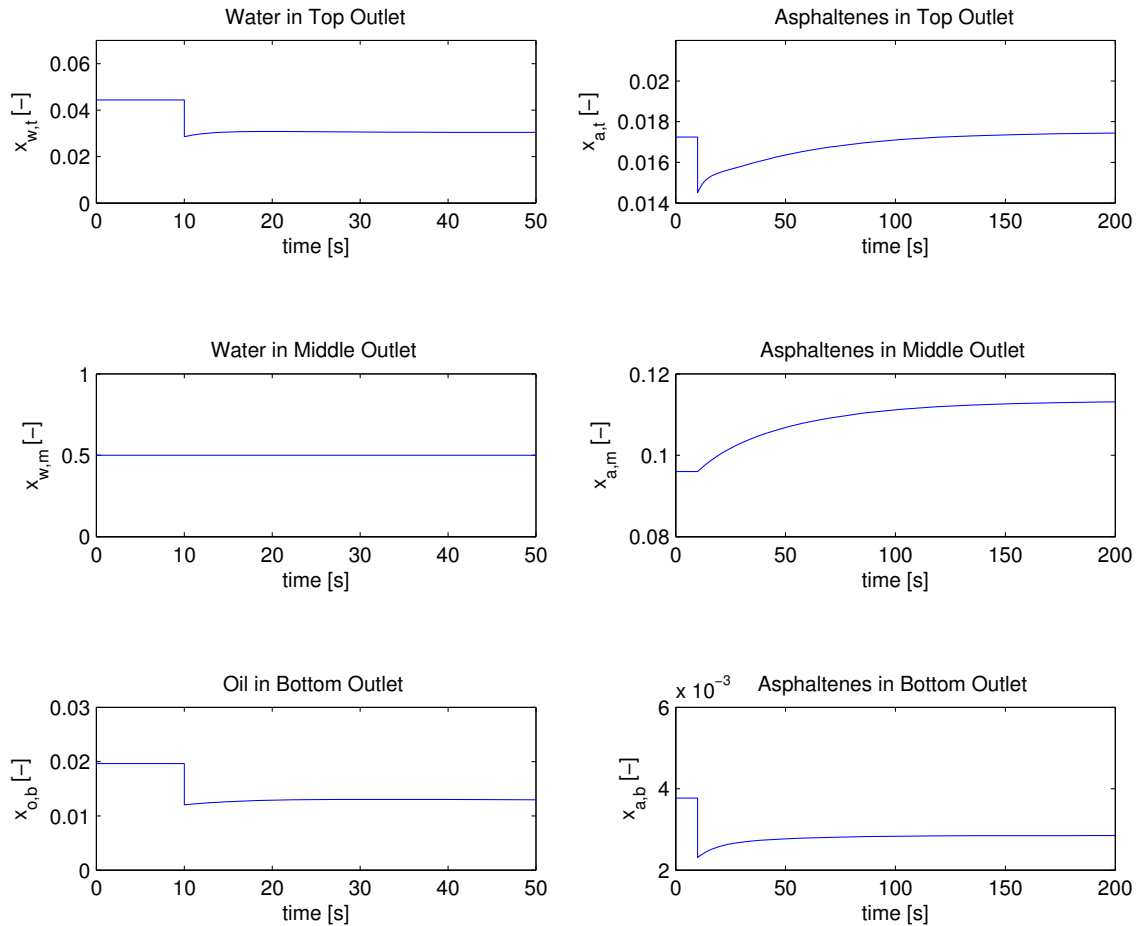


Figure 16: Simulated response of a 5 % decrease in feed rate. The left hand side are the water and oil impurities of the outlet streams. The right hand side show the asphaltene content of each output stream.

The model shows a behavior that seems reasonable, but it needs verification in form of comparison with experimental data. The main questions to be answered is how the characteristic droplet size can be correlated to known properties of the inlet emulsion, and how the asphaltenes are distributed in the separator, and how they affect the separation rate.

4.1.1 Impact of Characteristic Drop Size

As mentioned earlier, the choice of the characteristic drop size has a huge influence on the modeled performance of the separator. To demonstrate this, the steady state values of

the unwanted phase in the top and bottom outlets are presented in Table 4 for different characteristic drop sizes. The separator is modeled as described by Table 1, 2 & 3, except for the declining characteristic droplet radius, r_d . The separation decreases significantly with r_d and there is almost no separation when $r_d = 100 \mu m$ (the inlet water cut is 50 %). Keep in mind that $100 \mu m$ is not a very small radius for a droplet in this kind of system. Having a method for predicting the characteristic drop size therefore becomes vital in order for the model to accurately predict the separation performance. The effect of other physical parameters on the separation efficiency is listed in Appendix B.

Table 4: Impact of characteristic drop size on separation

Char. droplet radius [μm]	Oil in bottom outlet [vol%]	Water in top outlet [vol%]
250	2	4
200	12	17
150	29	27
100	42	35

4.2 Swirl Separator

The physical parameters of the swirl separator are listed in Table 5. The dimensions of the separator are chosen based on being able to handle the bottom outlet of the gravity separator described in section 4.1. The proportionality constant, k , between the angular frequency and the volumetric flow rate is set to $160 \frac{rad/s}{m^3/s}$. This corresponds to a maximum angular velocity of about 6 times the average axial velocity, and is based on the same ratio measured by van Campen et al. in a similar experimental setup [?].

The desirable ratio between the inner pipe, R_i , and the outer pipe, R , depends on the operational objective of the separator. It is assumed that the main objective for the separator is to purify the water phase in the heavy phase outlet, HPO. It is then necessary to have a split ratio between the LPO and HPO (Split Ratio= $(R_i/R)^2$) that is greater than the maximum inlet volume fraction of oil. This is to avoid that the cylindrical continuous oil phase is wider than the inner outlet pipe. The concept is explained with Figure 13 in section 3.2. The split ratio is set to 0.03, which means that the HPO can be completely free of oil for inlet flows with oil volume fractions up to 3 %.

Table 5: Physical parameters of the swirl separator

Symbol	Description	Value	Unit
L_{sw}	Length of separator	4.6	m
R	Radius of separator (outer pipe)	20	cm
R_i	Radius of inner pipe (LPO)	3.5	cm
k	Proportionality constant (equation 3.22)	160	$\frac{rad/s}{m^3/s}$

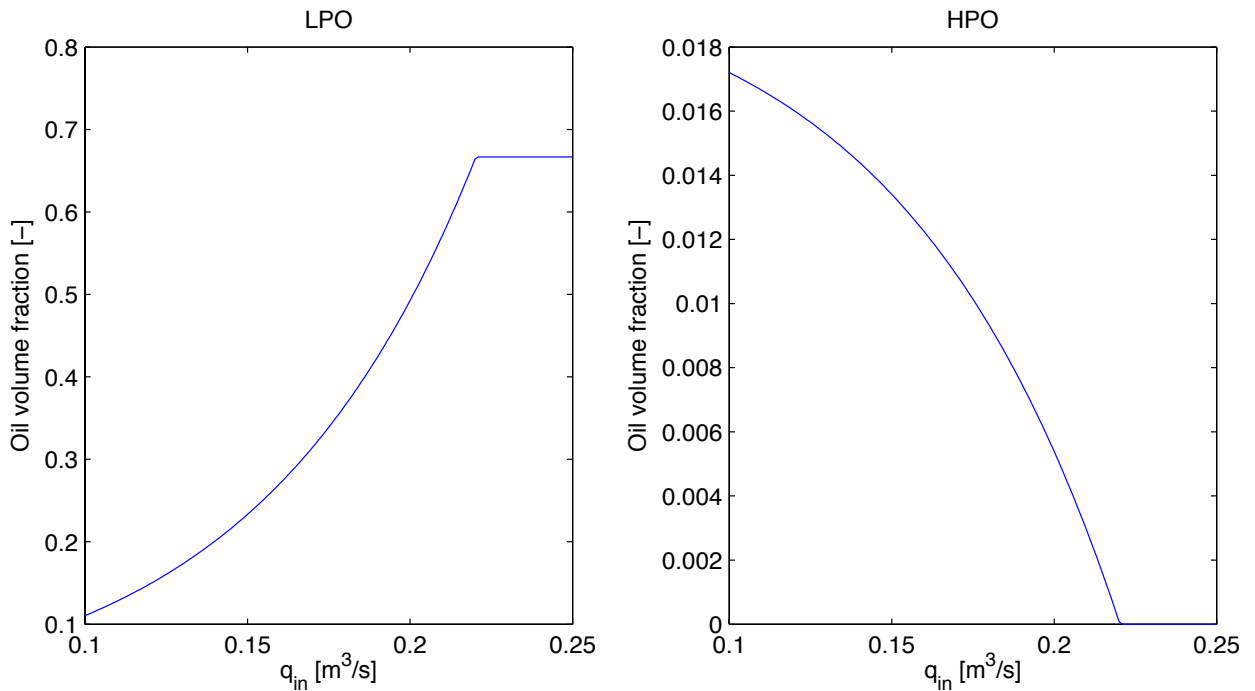
It is reasonable to believe that the oil droplets in the bottom outlet of the gravity separator is in the lower section of the droplet size distribution. The characteristic droplet radius of the swirl separator is therefore set to 10 % of the value used for the gravity separator. The properties of the inlet fluid are listed in Table 6, the properties that are unchanged from to the gravity separator can be found in Table 1.

Table 6: Physical properties of the emulsion in the swirl separator

Symbol	Description	Value	Unit
r_d	Characteristic droplet radius	25	μm
$x_{a,in}$	Volume fraction of asphaltenes in inlet	0.0038	—
$x_{o,in}$	Volume fraction of oil in inlet	0.02	—

The swirl separator was simulated for an increasing inlet flow rate. The oil volume fractions in the two outlets are presented in Figure 17. The degree of separation increases as a result of the increasing centrifugal acceleration. The centrifugal acceleration is highest at the radius of the "solid body rotation" core, R_c , and increases from about 50 times the gravitational acceleration, g , for the lowest flow rate to about 300 g for the highest. This is in the expected magnitude for this kind of separator [9].

The LPO flow reaches a maximum oil content at $0.22 \text{ m}^3/s$ as a result of the fixed split between the two outlet flows. This unwanted behavior, motivates the desire to manipulate the ratio between the LPO and HPO flow rates. This implies that there will be a gradient in the axial velocity field around the radius of the inner pipe and the behavior of the fluid will become even harder to predict.

**Figure 17:** The volume fraction of oil in the light- (left) and heavy- (right) phase outlet versus the inlet volumetric flow rate.

4.2.1 Effect of the Flow Rate on Separation

The model gives increased separation for increasing inlet flow rates. This seems reasonable as the swirl flow is driven by the flow through the swirl element. It is, however, likely that there will be a point where the damaging effect of the high flow rate becomes more dominant than the positive effects. This section discusses how deviations from the model assumptions can effect the predicted separation.

The model assumes a linear relationship between the volumetric flow rate and the angular frequency (equation 3.22). The linear relationship corresponds to the drag coefficient being inversely proportional to the Reynolds number. A Moody diagram, which verifies this assumption for low Reynolds numbers, is attached in Appendix C. This correlation is, however, not valid for high Reynolds numbers. It is hard to determine the behavior of the fluid around the swirl element, but an investigation of how a non-linear relationship would affect the separation has been executed.

The red curve on the left hand side in Figure 18 shows the relationship between the angular frequency and inlet flow rate with the original assumption. The blue curve shows a constructed relationship where the constant k , in equation 3.22 is replaced by a decaying factor. The right hand side shows the relative radius r_{in}/R , from equation 3.31, which is a measure for the degree of separation. The simulations show that the degree of separation reaches a maximum for the non-linear situation. Complete separation can still be reached, but the length of the separator will have to be increased. Which of the two cases that represent reality best for the respective flow rates is hard to say, but could be determined if the right experimental data becomes available in the future.

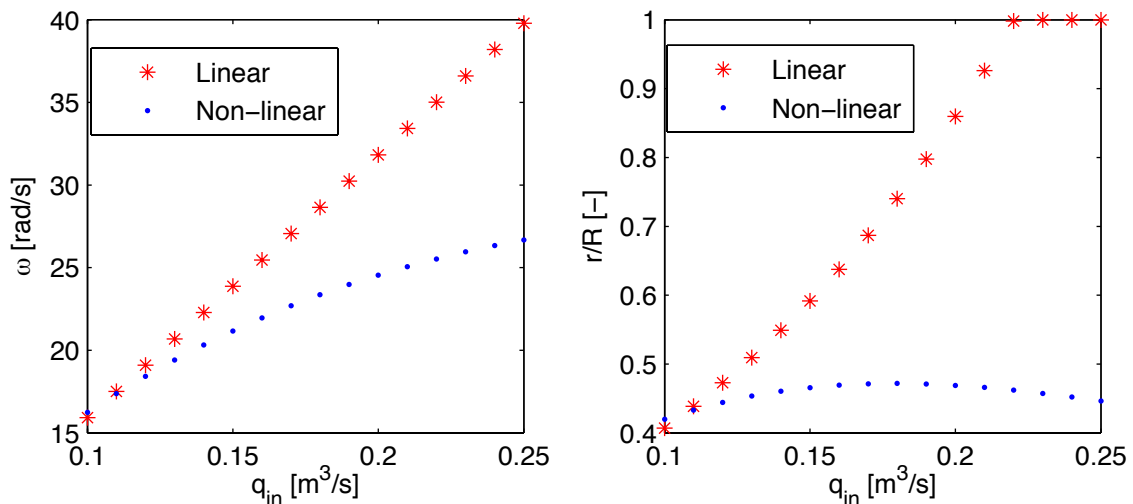


Figure 18: Effect of angular velocity on degree of separation. **Left:** Linear and non-linear relationship between angular frequency and volumetric flow rate. **Right:** All droplets that are within the radius r at the separator inlet will exit at the LPO. r/R is thus a measure for the degree of separation.

4.3 Combined System

A simulation was done where the two separators described above were combined by having the bottom out flow of the gravity separator as the inlet to the swirl separator. The flow diagram is presented in Figure 19. This configuration is meant to remove as much oil and asphaltenes as possible from the produced water in order to make it suitable for re-injection or release. Since the gravity separator is designed only to do the bulk separation, the oil rich product will contain significant amounts of water. This impurity can be reduced by having another swirl separator on the top and middle outlet of the gravity separator, but is not included for these simulations.

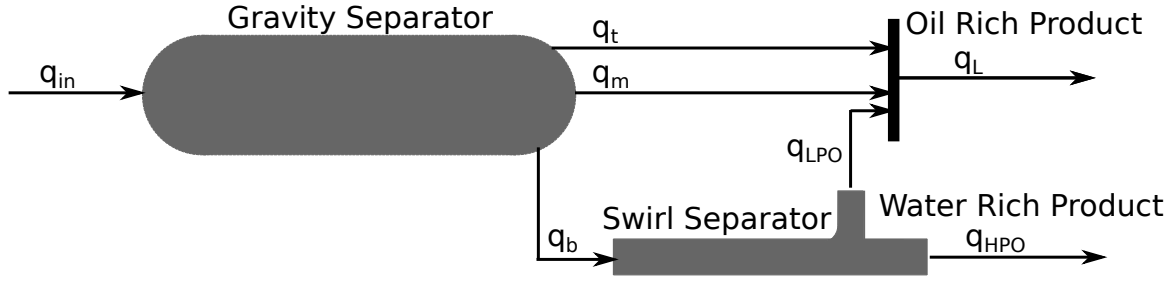


Figure 19: The bottom product from the gravity separator is sent to the swirl separator where the remaining oil is removed and recombined with the light phase.

The same 5 % step change in the inlet flow as in section 4.1 was introduced to the combined separation system. The response can be seen in Figure 20. The increasing separation capacity of the swirl separator for increasing flow rates counteracts the decreasing performance of the gravity separator. This results in an oil free heavy phase product, see graph of oil volume fraction versus time in Figure 20. This result is highly dependent on the correctness of the assumption about the linear relationship between the angular velocity and the inlet flow rate. If this assumption is inaccurate, it may result in a decreased purity of the heavy phase product as discussed in section 4.2.1.

The two bottom graphs show that most of the asphaltenes exit with the combined light phases, which seems reasonable as it contains most of the droplets. Low asphaltene concentrations in the produced water will in many cases be desirable to avoid re-injecting or releasing large amount of asphaltenes to the sea.

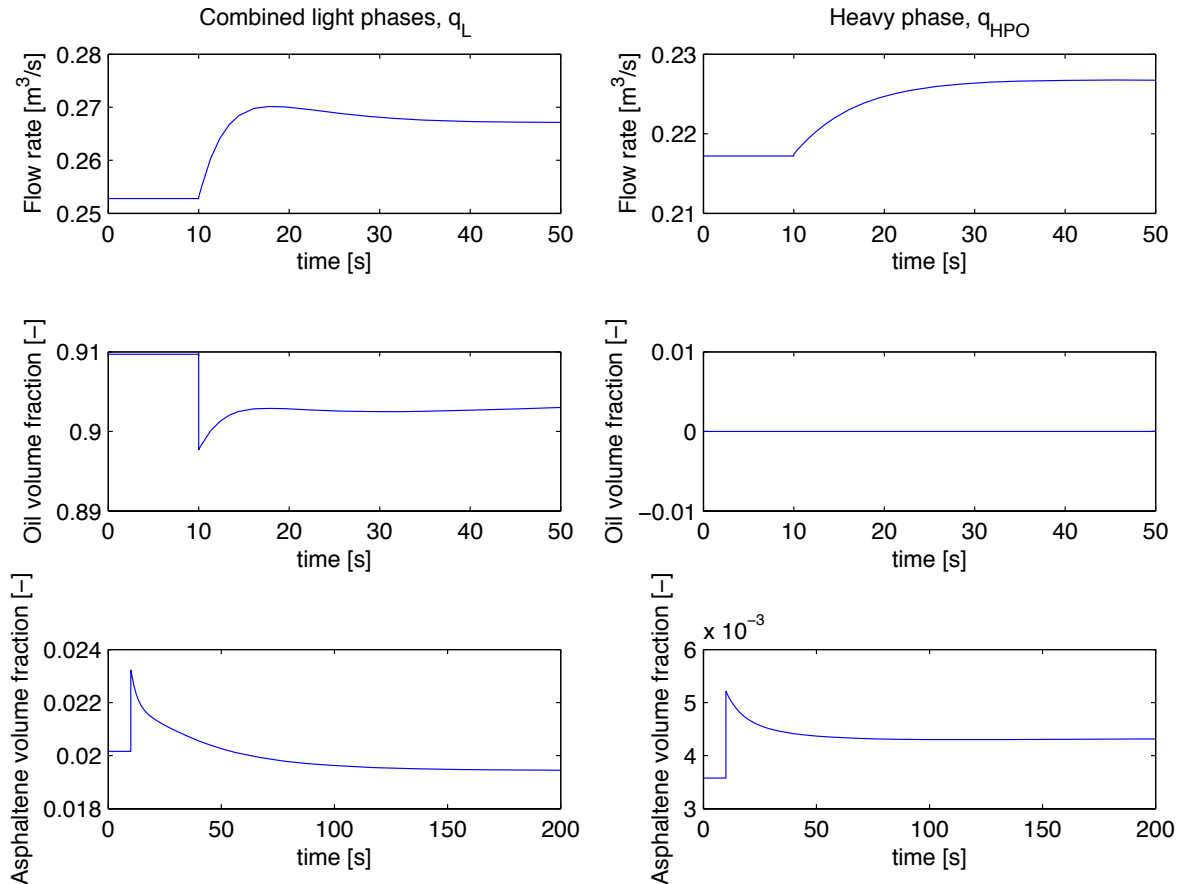


Figure 20: The response of the system for a 5 % increase in inlet flow rate. **Left:** Combined oil rich product, $q_L = q_t + q_m + q_{LPO}$. **Right:** Water rich product, q_{HPO} .

5 Conclusion

The modeled separators give reasonable responses to changes in the input parameters (e.g. flow rate, droplet size etc.). They do, however, require that these parameters are known for that particular system. The characteristic drop size is hard to estimate and other parameters (e.g. viscosities, densities etc.) will change during the life time of the oil field. Considering the simplicity of the models, they seem to give plausible predictions of the behavior of the respective separators.

The swirl separator model gives increased separation for greater inlet flow rates. This seems reasonable as the rotation is driven by the flow through the swirl element. On the other hand, it is likely that the separation efficiency will reach a maximum where the damaging effect of the high flow rate becomes more dominant on the separation than the increased centrifugal force. Finding this turning point is vital for optimization purposes and should be possible to do through experiments.

Both models are rather simplistic estimations of the real world and the accuracy will have to be evaluated based on experimental data, or through comparison with a more advanced model with known robustness and accuracy.

References

- [1] FMC Technologies, *InLine DeWaterer* , Available at: <http://fmctechnologies.com/en/SeparationSystems/Technologies/InLineTechnologies/InLineLiquidLiquidSeparation/InLineDeWaterer.aspx> (Last visited 28. November 2014)
- [2] FMC Technologies, *InLine ElectroCoalescer*, Available at: <http://fmctechnologies.com/en/SeparationSystems/Technologies/InLineTechnologies/InLineLiquidLiquidSeparation/InLineElectroCoalescer.aspx> (Last visited 30. November 2014)
- [3] FMC Technologies, *PipeSeparator*, Available at: <http://www.fmctechnologies.com/en/SeparationSystems/Technologies/SpecialSeparatorSolutions/PipeSeparator.aspx> (Last visited 28. November 2014)
- [4] Grimes, B. A. (2012) 'Population Balance Model for Batch Gravity Separation of Crude Oil and Water Emulsions. Part I: Model Formulation', *Journal of Dispersion Science and Technology*, 33:4, 578-590.
- [5] Grimes, B. A. et al. (2012) 'Population Balance Model for Batch Gravity Separation of Crude Oil and Water Emulsions. Part II: Comparison to Experimental Crude Oil Separation Data', *Journal of Dispersion Science and Technology*, 33:4, 591-598.
- [6] Mørk, P.C. (2004) *Overflate og Kolloidkjemi*, Institutt for kjemisk prosesssteknologi, 8. ed.
- [7] Orłowski, R. T. C. et al. (2012) *Marlim 3 Phase Subsea Separation System – Challenges and Solutions for the Subsea Separation Station to Cope with Process Requirements*, The Offshore Technology Conference held in Houston, Texas, 30 April–3 May 2012.
- [8] Sayda, A. F. and Taylor, J. H. (2007), *Modeling and Control of Three-Phase Gravity Separators in Oil Production Facilities*, Proceedings of the 2007 American Control Conference, New York, USA.
- [9] Slot, J. J. (2013), *Development of a Centrifugal In-Line Separator for Oil-Water Flows*, University of Twente, Netherlands.
- [10] Urdahl, O. et al. (1998) *Development of a New, Compact Electrostatic Coalescer Concept*, SPE Annual Technical Conference and Exhibition 27-30 September, 1998, New Orleans, Louisiana.
- [11] van Campen, L. J. A. M. et al. (2012) *An axial cyclone for oil/water separation*, Available at: <http://cheme.nl/tp/people/docs/LaurensPoster.pdf> (Last visited 28. November 2014)
- [12] Verginia Tech, *Moody Diagram*, Available at: www.dept.aoe.vt.edu/~jschetz/fluidnature/unit07/unit7f.html (Last visited 6. December 2014)
- [13] Westra, R. W. et al. (2011) *Compact Oil-water Separation using the InLine ElectroCoalescer and the Cyclonic DeWaterer*, The International Petroleum Technology Conference held in Bangkok, Thailand, 7–9 February 2012.
- [14] Yarranton, H. W. (1997), *Asphaltene Solubility and Asphaltene Stabilized Water-in-Oil Emulsions*, University of Alberta, Canada.

A MATLAB Code

A.1 Main Script

The main script solves the system of differential and algebraic equations given by the function *separation.m* for the desired input variables and plots the calculated response of the system.

```
1 clear all
2 clc
3
4 %Notation for variable a:
5 %a -Fixed value, da/dt=0 (M=1)
6 %a0 - Guess for variable, 0=x(j)-a (M=0)
7 %ai - Initial condition ,da/dt=eq. (M=1)
8
9 %-----Gravity Separator-----
10 Vwi=5.76; Voi=1.21; L10=1; L20=1.4; L1sp=1; L2sp=1.4;
11 elinti=0; e2inti=0;qin=0.335;eps0=1; qt0=qin/2-0.005;qb0=qin/2-0.005;
12 Vob0=0;Vwt0=0;qm=0.01;Vwm0=0; Vai=0.1;Vab0=0;Vat0=0.003;Vam0=0.1;
13 %-----Swirl separator for bottom outlet-----
14 Vol0=1;Voh0=0;q2h0=0.06;q2l0=0.03;Vai0=0.001;Vao0=0.001;
15 %-----
16
17 x0=[Vwi,Voi,L10,L20,L1sp,L2sp,elinti,e2inti,qin,eps0,qt0,qb0,Vob0,Vwt0,...
18      qm,Vwm0,Vai,Vab0,Vat0,Vam0...
19      Vol0,Voh0,q2h0,q2l0,Vai0,Vao0];
20 M=zeros(length(x0));
21 M(1,1)=1;
22 M(2,2)=1;
23 M(5,5)=1;
24 M(6,6)=1;
25 M(7,7)=1;
26 M(8,8)=1;
27 M(9,9)=1;
28 M(15,15)=1;
29 M(17,17)=1;
30
31 options = odeset('Mass',M);
32 %Calculate steady state at complete separation
33 [T,X]=ode15s(@separation,[0 10000],x0,options);
34 x0=X(end,:);
35 %New nominal steady state
36 x0(1,9)=0.47;
37 [T,X]=ode15s(@separation,[0 1000],x0,options);
38 x1=X(end,:);
39 %%
40 clc
41 [T1,X1]=ode15s(@separation,[0 10],x1,options);
42 x2=X1(end,:);
43 %Introducing a step
44 x2(1,9)=1.05*x2(1,9);
45 x2(1,15)=1.05*x2(1,15);
46 [T2,X2]=ode15s(@separation,[10 200],x2,options);
47 X=[X1;X2];
48 T=[T1;T2];
49
50 qin=X(:,9);qt=X(:,11);qb=X(:,12);qm=X(:,15);Vwm=X(:,16);Vam=X(:,20);
51 Vwt=X(:,14);Vat=X(:,19);Vob=X(:,13);Vab=X(:,18);
```

```

52 wc=0.5;
53
54 qHPO=X(:,23);qLPO=X(:,24);VoLPO=X(:,21);VoHPO=X(:,22);VaLPO=X(:,25);
55 VaHPO=X(:,26);
56
57 figure(1)
58
59 subplot(321)
60 plot(T,Vwt)
61 ylabel('x_{w,t} [-]')
62 xlabel('time [s]')
63 title('Water in Top Outlet ')
64 axis([0 50 0 0.07 ])
65
66 subplot(323)
67 plot(T,Vwm)
68 ylabel('x_{w,m} [-]')
69 xlabel('time [s]')
70 title('Water in Middle Outlet ')
71 axis([0 50 0 1 ])
72
73
74 subplot(325)
75 plot(T,Vob)
76 ylabel('x_{o,b} [-]')
77 xlabel('time [s]')
78 title('Oil in Bottom Outlet ')
79 axis([0 50 0 0.03 ])
80
81 subplot(322)
82 plot(T,Vat)
83 ylabel('x_{a,t} [-]')
84 xlabel('time [s]')
85 title('Asphaltenes in Top Outlet ')
86 axis([0 200 0.014 0.022])
87
88 subplot(324)
89 plot(T,Vam)
90 ylabel('x_{a,m} [-]')
91 xlabel('time [s]')
92 title('Asphaltenes in Middle Outlet ')
93 axis([0 200 0.08 0.12])
94
95 subplot(326)
96 plot(T,Vab)
97 ylabel('x_{a,b} [-]')
98 xlabel('time [s]')
99 title('Asphaltenes in Bottom Outlet ')
100 axis([0 200 0.002 0.006])
101
102 figure(2)
103 subplot(221)
104 %Combined light phases: qL
105 qL=qt+qm+qLPO;
106 qoL=(1-Vwt-Vat).*qt+(1-Vwm-Vam).*qm+VoLPO.*qLPO;
107 qaL=Vat.*qt+Vam.*qm+VaLPO.*qLPO;
108 VoL=qoL./qL;
109 VaL=qaL./qL;
110
111 subplot(321)

```

```

112 plot(T,qL)
113 xlabel('time [s]')
114 ylabel('Flow rate [m^3/s]')
115 title('Combined light phases, q_L')
116 subplot(322)
117 plot(T,qHPO)
118 xlabel('time [s]')
119 ylabel('Flow rate [m^3/s]')
120 title('Heavy phase, q_{HPO}')
121 subplot(323)
122 plot(T,VoL)
123 xlabel('time [s]')
124 ylabel('Oil volume fraction [-]')
125 subplot(324)
126 plot(T,VoHPO)
127 xlabel('time [s]')
128 ylabel('Oil volume fraction [-]')
129 subplot(325)
130 plot(T,VaL)
131 xlabel('time [s]')
132 ylabel('Asphaltene volume fraction [-]')
133 subplot(326)
134 plot(T,VaHPO)
135 xlabel('time [s]')
136 ylabel('Asphaltene volume fraction [-]')
137 %%
138 clc
139 [T1,X1]=ode15s(@separation,[0 10],x1,options);
140 x2=X1(end,:);
141 x2(1,9)=0.95*x2(1,9);
142 x2(1,15)=0.95*x2(1,15);
143 [T2,X2]=ode15s(@separation,[10 200],x2,options);
144
145 X=[X1;X2];
146 T=[T1;T2];
147
148 qin=X(:,9);qt=X(:,11);qb=X(:,12);qm=X(:,15);Vwm=X(:,16);Vam=X(:,20);
149 Vwt=X(:,14);Vat=X(:,19);Vob=X(:,13);Vab=X(:,18);
150 wc=0.5;
151
152 figure(3)
153 subplot(321)
154 plot(T,Vwt)
155 ylabel('x_{w,t} [-]')
156 xlabel('time [s]')
157 title('Water in Top Outlet ')
158 axis([0 50 0 0.07 ])
159
160 subplot(323)
161 plot(T,Vwm)
162 ylabel('x_{w,m} [-]')
163 xlabel('time [s]')
164 title('Water in Middle Outlet ')
165 axis([0 50 0 1 ])
166
167
168 subplot(325)
169 plot(T,Vob)
170 ylabel('x_{o,b} [-]')
171 xlabel('time [s]')

```

```

172 title('Oil in Bottom Outlet ')
173 axis([0 50 0 0.03 ])
174
175 subplot(322)
176 plot(T,Vat)
177 ylabel('x_{a,t} [-]')
178 xlabel('time [s]')
179 title('Asphaltenes in Top Outlet ')
180 axis([0 200 0.014 0.022])
181
182 subplot(324)
183 plot(T,Vam)
184 ylabel('x_{a,m} [-]')
185 xlabel('time [s]')
186 title('Asphaltenes in Middle Outlet ')
187 axis([0 200 0.08 0.12])
188
189 subplot(326)
190 plot(T,Vab)
191 ylabel('x_{a,b} [-]')
192 xlabel('time [s]')
193 title('Asphaltenes in Bottom Outlet ')
194 axis([0 200 0.002 0.006])
195 %%
196 clc
197 [T1,X1]=ode15s(@separation,[0 10],x1,options);
198 x2=X1(end,:);
199 x2(1,9)=1.0*x2(1,9);
200 x2(1,15)=1.0*x2(1,15);
201 [T2,X2]=ode15s(@separation,[10 200],x2,options);
202 X=[X1;X2];
203 T=[T1;T2];
204
205 Qin=X(:,9);qt=X(:,11);qb=X(:,12);qm=X(:,15);Vwm=X(:,16);Vam=X(:,20);
206 Vwt=X(:,14);Vat=X(:,19);Vob=X(:,13);Vab=X(:,18);
207 wc=0.5;
208
209 qHPO=X(:,23);qLPO=X(:,24);VoLPO=X(:,21);VoHPO=X(:,22);VaLPO=X(:,25);
210 VaHPO=X(:,26);
211
212 figure(1)
213
214 subplot(321)
215 plot(T,Vwt)
216 ylabel('x_{w,t} [-]')
217 xlabel('time [s]')
218 title('Water in Top Outlet ')
219 axis([0 50 0 0.07 ])
220
221 subplot(323)
222 plot(T,Vwm)
223 ylabel('x_{w,m} [-]')
224 xlabel('time [s]')
225 title('Water in Middle Outlet ')
226 axis([0 50 0 1 ])
227
228
229 subplot(325)
230 plot(T,Vob)
231 ylabel('x_{o,b} [-]')

```

```

232 xlabel('time [s]')
233 title('Oil in Bottom Outlet ')
234 axis([0 50 0 0.03 ])
235
236 subplot(322)
237 plot(T,Vat)
238 ylabel('x_{a,t} [-]')
239 xlabel('time [s]')
240 title('Asphaltenes in Top Outlet ')
241 axis([0 200 0.014 0.022])
242
243 subplot(324)
244 plot(T,Vam)
245 ylabel('x_{a,m} [-]')
246 xlabel('time [s]')
247 title('Asphaltenes in Middle Outlet ')
248 axis([0 200 0.08 0.12])
249
250 subplot(326)
251 plot(T,Vab)
252 ylabel('x_{a,b} [-]')
253 xlabel('time [s]')
254 title('Asphaltenes in Bottom Outlet ')
255 axis([0 200 0.002 0.006])
256
257 figure(2)
258 subplot(221)
259 %Combined light phases: qL
260 qL=qt+qm+qLPO;
261 qoL=(1-Vwt-Vat) .*qt+(1-Vwm-Vam) .*qm+VoLPO .*qLPO;
262 qaL=Vat .*qt+Vam .*qm+VaLPO .*qLPO;
263 VoL=qoL./qL;
264 VaL=qaL./qL;
265
266 subplot(321)
267 plot(T,qL)
268 xlabel('time [s]')
269 ylabel('Flow rate [m^3/s]')
270 title('Combined light phases, q_L')
271 subplot(322)
272 plot(T,qHPO)
273 xlabel('time [s]')
274 ylabel('Flow rate [m^3/s]')
275 title('Heavy phase, q_{HPO}')
276 subplot(323)
277 plot(T,VoL)
278 xlabel('time [s]')
279 ylabel('Oil volume fraction [-]')
280 subplot(324)
281 plot(T,VoHPO)
282 xlabel('time [s]')
283 ylabel('Oil volume fraction [-]')
284 subplot(325)
285 plot(T,VaL)
286 xlabel('time [s]')
287 ylabel('Asphaltene volume fraction [-]')
288 subplot(326)
289 plot(T,VaHPO)
290 xlabel('time [s]')
291 ylabel('Asphaltene volume fraction [-]')

```

A.2 Separation System Function: separation.m

The function *separation.m* contains the equations of the models for the gravity- and swirl separators.

```
1 function DXDT=separation(t,x)
2 %Notation:
3 %Vi: Total volume of phase i
4 %Vij: Voulume fraction of i in stream j
5 %xij=Vij
6 %Subscript: t=top outlet, m=middle outlet, b= bottom outlet
7 %           a=asphaltene, w=water, o=oil
8
9 %-----Gravity Separator-----
10 %Gravity separator dimension
11 lsep=4.6; %m
12 Rsep=0.75;
13 Vsep=pi*Rsep^2*lsep;
14
15 %Defining variables
16 Vw=x(1);
17 Vo=x(2);
18 h=x(3);           %Level 1
19 L2=x(4);           %Level 2
20 L1sp=x(5);
21 L2sp=x(6);
22 elint=x(7);
23 e2int=x(8);
24 qin=x(9);
25 qm=x(15);
26 Va=x(17);
27
28 %Physical parameters
29 rd=250*10^-6;      %m^3
30 rhoo=900;          %kg/m^3
31 rhow=1000;
32 muw=0.467*10^-3; %Pa*s
33
34 qin0=0.335;        %m^3/s
35 qt0=0.5*(qin0-qm);
36 qb0=qin0-qt0;
37 wc=0.5;
38 sc=0.025;
39
40 vv=(2/9)*9.81*(rhow-rhoo)*rd^2/muw;
41 vh=lsep*wc*qin/Vw;
42
43 phil=atan(vv/vh);
44
45 h1=lsep*tan(phi1);
46
47 l1=h/tan(phi1);
48 theta=acos(1-h/Rsep);
49 thetal=acos(1-h1/Rsep);
50 VS1=Rsep^2*l1*(theta-0.5*sin(2*theta)-...
51     (3*sin(theta)-3*theta*cos(theta)-sin(theta)^3)...
52     /(3*(1-cos(theta))));
53 VS2=Rsep^2*lsep*(theta-0.5*sin(2*theta)-...
54     (3*sin(thetal)-3*thetal*cos(thetal)-sin(thetal)^3)...
```

```

55     / (3 * (1 - cos(theta1))) );
56 if l1 > lsep
57     eps = 1 - VS2 / VS1;
58 else
59     eps = 0;
60 end
61
62 %Controller
63 e1 = L1sp - h;
64 Kc1 = -1;
65 tau1 = 70;
66 e2 = L2sp - L2;
67 Kc2 = -1;
68 tau2 = 70;
69 qb = qb0 + Kc1 * (e1 + e1int / tau1);
70 qt = qt0 + Kc2 * (e2 + e2int / tau2);
71
72
73 %Split of unseparated liquid
74 T = 1.3;
75 B = 0;
76 M = 1;
77 ft = (h1 - B) / (h1 - B + T - h);
78 if h > T
79     display('Unseparated in top outlet')
80     return
81 end
82
83 %Mass balances
84 qo1 = eps * (1 - wc) * qin;
85 qw1 = eps * wc * qin;
86 qo2 = (1 - eps) * (1 - wc) * qin;
87 if (qo1 + qw1) <= qm
88     qo1 = 0;
89     qw1 = 0;
90 else
91     qo1 = qo1 - (1 - wc) * qm;
92     qw1 = qw1 - wc * qm;
93 end
94 dVwdt = qin - qb - qo2 - qm - ft * (qo1 + qw1); %Continuous water phase
95 dVodt = qo2 - (qt - ft * (qo1 + qw1)); %Continuous oil phase
96
97 xab = 0.9 * 3 * Va / Vw; %A in unseparated oil to bottom
98 xat = 0.9 * 3 * Va / Vw; %A in unseparated oil to top
99 qaot = 0.1 * (Va / Vo) * (qt - ft * (qo1 + qw1)); %A solved in oil phase
100 qam = 0.9 * 3 * Va / Vw * qm; %Assuming h=M
101 dVadt = sc * (1 - wc) * qin - qam... %Asphaltenes (A) in- A in qm
102     - qaot - xab * (1 - ft) * (qo1 + qw1) - xat * ft * (qo1 + qw1);
103
104 res1 = (Rsep^2 / 2) ...
105     * (2 * acos(1 - h / Rsep) - sin(2 * acos(1 - h / Rsep))) ...
106     - (Vw) / lsep;
107 res2 = (Rsep^2 / 2) ...
108     * (2 * acos(1 - L2 / Rsep) - sin(2 * acos(1 - L2 / Rsep))) ...
109     - (Vo + Vw) / lsep;
110
111 %Purities
112 Vab = xab * (1 - ft) * (qo1 + qw1) / qb;
113 Vat = (xat * ft * (qo1 + qw1) + qaot) / qt;
114 Vam = 0.9 * 3 * Va / Vw;

```

```

115 Vob=(1-ft)*qo1/qb;
116 Vwt=ft*qw1/qt;
117 if (qo1+qw1)≤qm
118     Vwm=1-Vam;
119 else
120     Vwm=wc;
121
122 end
123 %-----
124
125 %-----Swirl separator for bottom outlet-----
126 R2o=0.2;
127 Lsw=2;
128 Split=0.03;           %qlightpase/qin
129 R2i=sqrt(Split)*R2o;
130
131 rds=0.1*rd; %25*10-6;
132
133 Rc=0.25*R2o;
134 va=qb/(pi*R2o2);
135 k=20;
136 w=k*va;           %angular frequency of core
137
138 q2i=Split*qb;       %Light phase out flow
139 q2o=qb-q2i;        %Heavy phase out flow
140
141 %Asphaltenes
142 Vai=(3-2*R2i/R2o)*Vab;
143 Vao=(Vab*qb-Vai*q2i)/q2o;
144
145 %Separation
146 ta=pi*R2o2*Lsw./qb;
147 alpha=2/9*(rhoo-rhow)*rds2/muw;
148 r=Rc*exp(-alpha*(2*pi*w)2*ta+(R2i2/Rc2-1)/2);
149
150 if r>R2o
151     r=R2o;
152 end
153 %Oil
154 Voi=(r/R2o)2*Vob*qb/q2i;
155 if Voi>1
156     Voi=1-Vai;
157 end
158
159 Voo=(Vob*qb-Voi*q2i)/q2o;
160
161
162 %-----
163
164
165 %-----Gravity Separator-----
166 DXDT(1)=dVwdt; DXDT(2)=dVodt; DXDT(3)=res1; DXDT(4)=res2;
167 DXDT(5)=0; DXDT(6)=0; DXDT(7)=e1; DXDT(8)=e2; DXDT(9)=0;
168 DXDT(10)=x(10)-eps; DXDT(11)=x(11)-qt; DXDT(12)=x(12)-qb;
169 DXDT(13)=x(13)-Vob; DXDT(14)=x(14)-Vwt;DXDT(15)=x(15)-qm;
170 DXDT(16)=x(16)-Vwm; DXDT(17)=dVadt; DXDT(18)=x(18)-Vab;
171 DXDT(19)=x(19)-Vat; DXDT(20)=x(20)-Vam;
172 %-----Swirl separator for bottom outlet-----
173 DXDT(21)=x(21)-Voi;DXDT(22)=x(22)-Voo;DXDT(23)=x(23)-q2o;
174 DXDT(24)=x(24)-q2i;DXDT(25)=x(25)-Vai;DXDT(26)=x(26)-Vao;

```

```

175
176 DXDT=DXDT';

```

A.3 Swirl Separator Script

The swirl separation script was used to calculate the separation efficiency for different flow rates.

```

1 %% Swirl Separator
2 R2o=0.2;
3 Split=0.03;                               %qlightpase/qin
4 R2i=sqrt(Split)*R2o;                       %Inner Radius
5
6 L=2;
7 qb=0.1:0.01:0.25;                          %Flow rate, m^3/s
8 Vob=0.02;                                   %Inlet volume fraction
9 Vab=0.0038;
10 rd=25*10^-6;                               %m^3
11 rhoo=900;                                  %kg/m^3
12 rhow=1000;
13 muw=0.467*10^-3;                          %Pa*s
14
15 %
16 Rc=0.25*R2o;
17 va=qb/(pi*R2o^2);
18 k=20;
19 w=k*va;                                     %Correlation used in model
20 w2=27*va.*exp(-2.8*qb);                   %Alternative correlation
21
22 ac=(2*pi*w*Rc).^2/Rc;
23 vtmax=2*pi*w*Rc;
24
25 %
26 q2i=Split*qb;                             %Light phase outflow
27 q2o=qb-q2i;                               %Heavy phase outflow
28
29 %
30 ta=pi*R2o^2*L./qb;
31 alpha=2/9*(rhoo-rhow)*rd^2/muw;
32 %Inlet radius of separated droplets
33 r=Rc*exp(-alpha*(2*pi*w).^2.*ta+(R2i^2/Rc^2-1)/2);
34 %Inlet radius for alternative w(q)
35 r2=Rc*exp(-alpha*(2*pi*w2).^2.*ta+(R2i^2/Rc^2-1)/2);
36
37 for i=1:length(r)
38     if r(i)>R2o
39         r(i)=R2o;
40     elseif r2(i)>R2o
41         r2(i)=R2o;
42     end
43 end
44 Voi=(r/R2o).^2*Vob.*qb./q2i;
45 Vai=Vab*(3-2*R2i/R2o);
46 for i=1:length(Voi)
47     if Voi(i)>1
48         Voi(i)=1-Vai;
49     end
50 end

```

```

51 Voo=(Vob.*qb-Voi.*q2i)./q2o;
52
53 %% Plotting Separation Efficiency
54 subplot(121)
55 plot(qb,Voi)
56 xlabel('q_{in} [m^3/s]')
57 ylabel('Oil volume fraction [-]')
58 title('LPO')
59 subplot(122)
60 plot(qb,Voo)
61 xlabel('q_{in} [m^3/s]')
62 ylabel('Oil volume fraction [-]')
63 title('HPO')
64 %% Separation Efficiency fo Alternative w(q)
65 subplot(121)
66 plot(qb,w,'r*');
67 hold on
68 plot(qb,w2,'. ');
69 ylabel('\omega [rad/s]')
70 xlabel('q_{in} [m^3/s]')
71 legend('Linear','Non-linear')
72 subplot(122)
73 plot(qb,r/R2o,'r*');
74 hold on
75 plot(qb,r2/R2o,'. ');
76 ylabel('r/R [-]')
77 xlabel('q_{in} [m^3/s]')
78 legend('Linear','Non-linear')

```

B Effect of Fluid Parameters on Separation

The effect of changing the physical parameters of the incoming fluid to the gravity separator on the quality of the top and bottom outlet flows are summarized in Table B.1-B.3. These parameters will differ from field to field and may change during the life time of a specific oil field. The bold rows represent the values used in the simulations in section 4.

Table B.1: Impact of characteristic drop size on separation

Char. Droplet Radius [μm]	Oil in Bottom Outlet [vol%]	Water in Top Outlet [vol%]
250	2	4
200	12	17
150	29	27
100	42	35

Table B.2: Impact of density on separation

$\rho_w - \rho_o$ [kg/m^3]	Oil in Bottom Outlet [vol%]	Water in Top Outlet [vol%]
50	20	22
80	6	11
100	2	4
120	0	0

Table B.3: Impact of water viscosity (temperature) on separation

Water Viscosity (Temp.) [$mPa \cdot s$]	Oil in Bottom Outlet [vol%]	Water in Top Outlet [vol%]
1.0 (20 °C)	22	23
0.65 (40 °C)	9	14
0.47 (60 °C)	2	4
0.36 (80 °C)	0	0

C Moody Diagram

The Moody diagram shows the relationship between the friction factor, wall roughness and Reynolds number for a pipe flow and is presented in Figure C.1. The non-linearity at high Reynolds number can have an impact on the angular velocity in swirl separator.

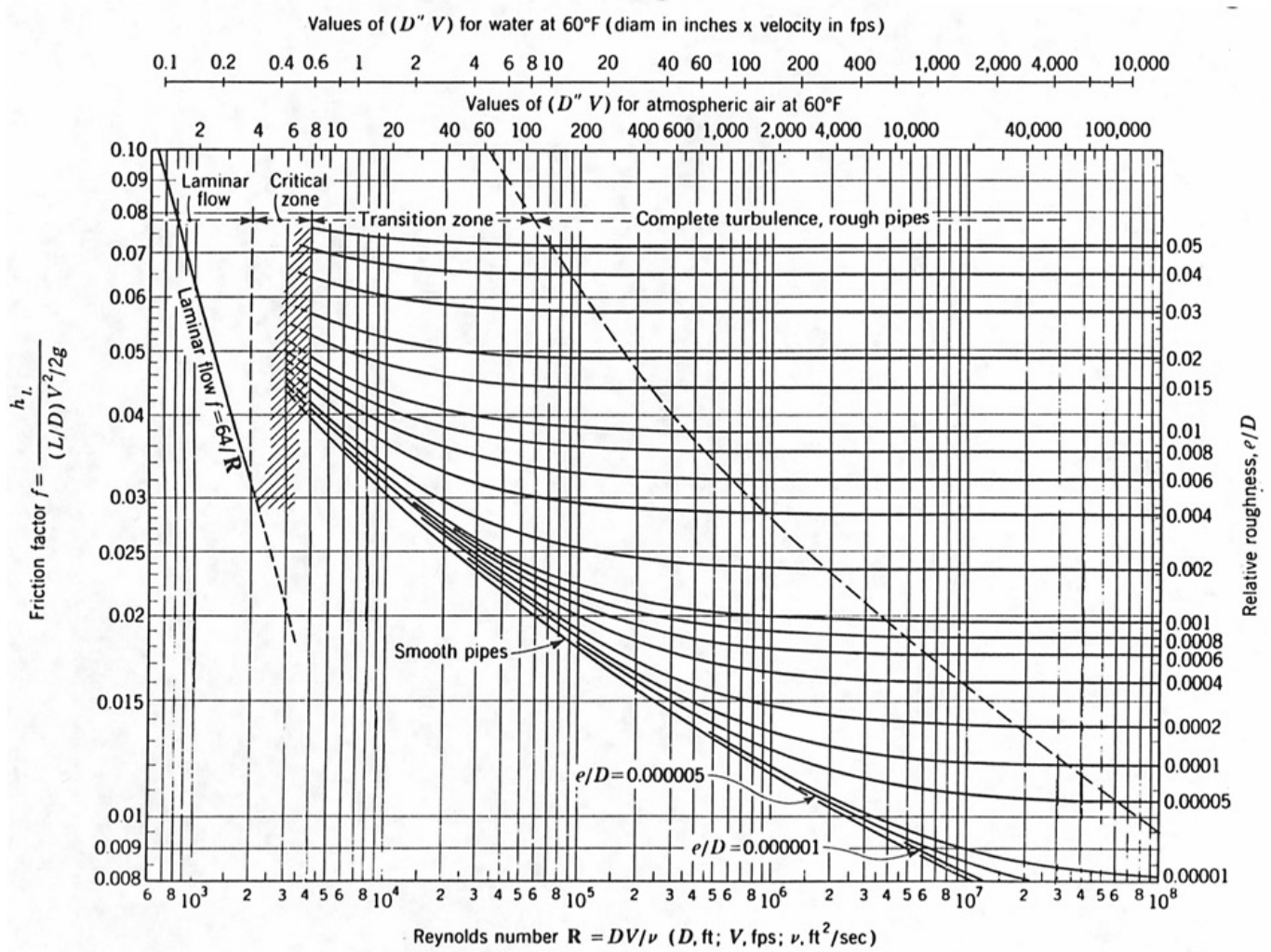


Figure C.1: The Moody diagram gives the relationship between the friction factor and the Reynolds number for a flow through a pipe. Adapted from a Virginia Tech homepage [12]